Universidade de Aveiro Departamento de Física

2018

Tiago Maurício de Pinho Leite

Soluções em fibra ótica para sistemas de reabilitação física e aplicações e-Health

Optical fiber solutions to physical rehabilitation systems and e-Health applications

Universidade de Aveiro Departamento de Física

2018

Tiago Maurício de Pinho Leite

Soluções em fibra ótica para sistemas de reabilitação física e aplicações e-Health

Optical fiber solutions to physical rehabilitation systems and e-Health applications

Dissertação apresentada à Universidade de Aveiro para cumprimento dos requisitos necessários à obtenção do grau de Mestre em Engenharia Física. Realizada sob a orientação científica do Doutor Paulo Fernando da Costa Antunes, Investigador Auxiliar da Universidade de Aveiro e do I3N, e da Doutora Maria de Fátima Fonseca Domingues, Investigadora de pós-Doutoramento do Instituto de Telecomunicações e do I3N.

O júri

Presidente	Prof. Doutor Manuel Almeida Valente Professor Associado do Departamento de Física da Universidade de Aveiro
Vogal - Arguente	Prof. Doutor Paulo Sérgio de Brito André Professor Associado com Agregação do Departamento de Engenharia Eletrotécnica e de Computadores, Instituto Superior Técnico, Universidade de Lisboa
Vogal - Orientador	Doutor Paulo Fernando da Costa Antunes Investigador Auxiliar da Universidade de Aveiro

agradecimentos

Pretendo expressar o meu agradecimento a todas as entidades que me ajudaram no desenvolvimento desta dissertação.

Aos meus orientadores Doutor Paulo Fernando da Costa Antunes e Doutora Maria de Fátima Fonseca Domingues pela orientação científica, disponibilidade e conhecimento transmitido.

Ao Departamento de Física da Universidade de Aveiro, Departamento de Mecânica da Universidade de Aveiro, I3N e ao Instituto de Telecomunicações – Pólo de Aveiro, pelas condições e material disponibilizado para a preparação e realização deste trabalho. Ao projeto WeHope, do Instituto de Telecomunicações, pela disponibilização de meios para a realização do trabalho.

Um agradecimento à Mestre Cátia Tavares que me acompanhou em todas as fases deste projeto e aos colegas com quem partilhei laboratório durante este ano. Aos Mestres Tiago Paixão e Alexandre Carvalho pela disponibilidade e apoio técnico. À Carlota Pereira pela ajuda na revisão ortográfica.

Aos Mestres José Ferreira e João Lucas Gomes pelo apoio e amizade.

Aos meus pais.

palavras-chave

Sensores em fibra-ótica, Rede Bragg em fibra ótica, Pressão plantar, Pressão de cisalhamento, Análise da marcha.

resumo

Nesta dissertação é proposto um sensor biaxial em fibra ótica, baseado em redes de Bragg, para monitorização simultânea de pressões plantar e de cisalhamento.

Este trabalho começa com a definição do problema: as consequências de patologias associadas ao pé diabético e distúrbios na sincronização dos membros inferiores. Foram analisados vários estudos publicados anteriormente sobre sensores de pressão plantar, as diversas metodologias e aplicações já existentes.
Foi realizada uma pesquisa na área da biomecânica, com particular foco no padrão de marcha e na anatomia do pé humano, de forma a compreender as diferentes fases da marcha e os pontos de maior interesse para monitorização da pressão do pé.
Assim, foi desenvolvido um estudo sobre a resposta de sensores baseados em redes de Bragg à pressão, em várias configurações de células sensoriais, culminando na integração desses sensores em palmilhas. Foram obtidas sensibilidades para pressão normal entre 0,56 e 2,16 pm/kPa e, para pressão de cisalhamento, entre 0,51 e 3,98 pm/kPa.
Estas demonstram ser uma solução não invasiva, com potencial de ser incluída em sistemas e-Health, para monitorização da marcha em tempo real. Podem ser preparadas para uso médico diário, servindo como importantes ferramentas no auxílio para a prevenção e diagnóstico, em especial de doenças do pé.

keywords

Optical Fiber Sensors, Fiber Bragg Grating, Plantar Pressure, Shear Pressure, Gait Analysis.

abstract

In this dissertation a biaxial optical fiber sensor, based on Bragg gratings, is proposed for simultaneous monitoring of plantar and shear pressures.

This work begins with the definition of the problem: the consequences of pathologies associated with diabetic foot and lower limbs disorders. It was analysed several previously published studies on plantar pressure sensors, the several methodologies and applications that already exist.
A biomechanical research was carried out, with particular focus on gait pattern and human foot anatomy, in order to understand the different gait phases and points of greatest interest for foot pressure monitoring.
Thus, the response of sensors based on Bragg gratings was studied in several configurations of sensing cells, then integrated in insoles. The sensitivities obtained for normal pressure were between 0.56 and 2.16 pm/kPa and, for shear pressure, between 0.51 and 3.98 pm/kPa.
Those prove to be a non-invasive solution with potential to be included in e-health systems for real-time gait monitoring. They can be prepared for daily medical use, serving as important tools in aiding prevention and diagnosis, especially of foot diseases.

Contents

List of figures

List of tables

List of acronyms and constants

Λ	Period of the Bragg grating
λ_B	Bragg wavelength
$\Delta\lambda_B$	Bragg wavelength shift
$\Delta\lambda_1$	Bragg wavelength shift of FBG 1
$\Delta\lambda_2$	Bragg wavelength shift of FBG 2
k_i	Wave-vector of incident light
k_f	Wave-vector of diffracted light
K	Grating wave-vector
K_ε	Sensitivity to strain variation
$\Delta\varepsilon$	Strain variation
n	Refractive index
n_{eff}	Effective modal refractive index
P_V	Plantar pressure (normal pressure)
P_S	Shear pressure (horizontal pressure)
R_F	Reflection coefficient
T	Temperature
ΔT	Temperature variation

3D	Three Dimensional
COP	Center Of Pressure
FBG	Fiber Bragg Grating
FSR	Force Sensitive Resistors
KrF	Krypton Fluoride
LED	Light Emitting Diode
OFS	Optical Fiber Sensor
PLA	Polylactic acid
PMSS	Peak of Maximum Shear Stress
PPP	Peak of Plantar Pressure
PVDF	Polyvinylidene Fluoride
RAM	Random Access Memory
UV	Ultraviolet

Chapter 1

1. Introduction

In this chapter, it is described the state of art in gait analysis and foot pressure monitoring. First, the basic concepts about the foot anatomy and human gait dynamics are introduced. It is known that irregular foot pressure and abnormal gait patterns are related to lower limbs pathologies, spine disorders and other skeletal muscle diseases. Also, *diabetes mellitus* and the consequent development of foot neuropathy are critically associated with abnormal foot's shear and plantar pressures [1–3]. For this reason, foot pressure monitoring is a topic of growing interest in the scientific community. Several authors have dedicated their efforts to the study of gait pattern, as well as to the design of devices to monitor movement, coordination, and forces involved in the walking process.

In this chapter are analyzed several devices for plantar pressure and shear measuring, previously reported, since the first electronic prototypes to the new configurations.

1.1. Foot anatomy and gait pattern

The foot is a fundamental element of the human locomotion and a complex anatomic structure of multiples bones and muscles. Walking, a primary activity of the human being, involves a series of coordinated movements between the components of the foot, ankle, knee and hip, in an anatomically complex synergy. During the walk, in order to propel the body forward, the foot is subject to perpendicular and coplanar pressures, in relation to the walking plane. Plantar pressure is related to all the pressure induced by body weight (gravitational force) and the ground reaction forces. Coplanar pressure, named in this document as shear pressure, is associated with the horizontal forces between the foot and the ground, that pushes the human body into a certain direction. When anomalous, these pressures are directly linked to the foot's tissues breakdown, often causing ulceration and other foot related lesions [2, 3].

The sole of the foot is divided into three main regions – hindfoot, midfoot and forefoot – which can be subdivided into more specific regions of interest, such metatarsal and toe (hallux) areas, **Figure 1.1 (a)**. In order to simplify the functional vision of the human foot, several authors point to areas such as the heel, midfoot, first metatarsal and toe (hallux) as critical areas for monitoring plantar and shear pressure. The information obtained in these regions is crucial for the understanding of the structure and the motion procedures of the foot and, consequently, the entire body posture and gait pattern [4–7].

The gait cycle can be described in two phases: *stance* – when the foot is in contact with the floor – and *swing*, when there is no contact between the foot and the floor [8–10]. The gait cycle begins in stance phase, from the moment when the heel reaches the floor and lasts until when the toe ceases the contact with the ground, setting the beginning the swing phase. For the study here analyzed, only the stance phase is relevant, since it represents the period of the gait cycle where the pressures are active. In **Figure 1.1 (b)** are represented the different stages of the stance phase.

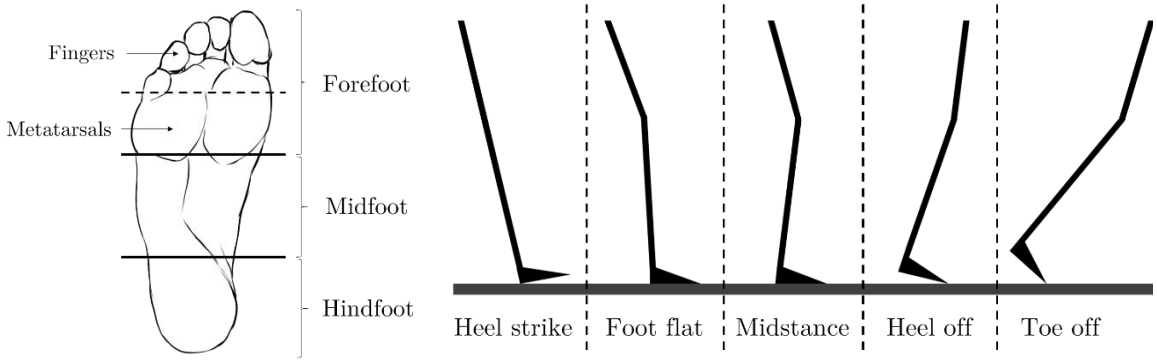

Figure 1.1– **(a)** Foot sole anatomy. **(b)** Scheme of the normal gait stance phase. *Adapted from Marasovic et al. 2009.*

In detail, the stance phase can be described by a succession of moments. The starting moment is characterized by the contact of the heel with the ground, the heel-strike. The second moment happens when the entire sole of the foot is in contact with the ground (foot flat). From this point, the body is pushed forward, as the hip surpasses the knee's plane, beginning the heel off. The stance phase continues until the foot leaves the contact with the ground (toe off).

In a normal subject, the stance phase can take up to 62% of the gait cycle time. Furthermore, in 12% of the gait time, the two feet are simultaneously in contact with the ground, in the *double support period,* which mirrors the level of synchronization between lower limbs and where the stance-swing phase transition is observed [2, 10, 11].

1.2. Problem statement

Diabetes mellitus is a group of metabolic disorders, characterized by the common condition of developing hyperglycemia [12, 13]. Long-term complications of *diabetes mellitus* may involve several organs, developing arterial insufficiency of lower limbs, gangrene and loss of pain sensation, leading to ulceration and consequent partial or full amputation of lower limb extremities [1, 3, 14–18]. The lifetime risk of a diabetic person to develop chronical peripheral neuropathy is 30 to 50% and the risk of ulceration can reach 25% [19-22]. Steinberg *et al.* points the diabetic foot ulcers as a major clinical problem with healing rate of barely 33% [23]. The financial costs associated to its treatment are considerably high, and it is therefore necessary to introduce foot care educational programs, special footwear and gait daily monitoring programs for the at-risk patients [1, 14, 23, 24].

Stroke survivors, obese and spine disorder patients, among others, may also experience several types of lower limb impairments, associated with muscle or neurological injuries. The recognition of anomalous plantar pressures – by specialized clinical analysis or integrated in a daily life wearables systems – may represent a serious advance in the alarm of cases of critical ulceration or even support physical therapy programs [2, 11, 25]. The demand of health monitoring systems in a world of fast technological and wireless communications development, allied to demographic shift, appoint e-Health systems as a feasible solution in this scenario. The market of non-invasive monitoring systems is growing significantly in response to the ageing and disability trend of the world population. These devices intend to reduce the number of lower limb-related pathologies, untreated due to lack of care and medical supervision, providing patients real-time control, while guaranteeing daily mobility [26–28].

1.3. State of art

In the last decades, gait and posture sensors have emerged along with the technological evolution. These devices had a crucial role in the gait pattern understanding of the gait pattern, being actively decisive in the clinical investigation of lower limbs diseases. Also, sports performance and biometric identification arise as areas of potential interest of these technologies. In the market, it can be found many electronic appliances for gait analysis – such pressure distribution platforms, imaging technologies and wearable in-shoe systems – equipped with piezoelectric, piezoresistive and capacitive sensors, among other electronic transducers.

In recent years, optical fibers changed the paradigm of sensor applications, especially in biomedical field. The intrinsic advantages and versatility of optical fibers made this technology a feasible alternative to electronic systems. The high sensitivity, small size, electromagnetic interference immunity, high accuracy, small drift and electrical isolation in the measuring point boost the optical fiber sensors (OFS) race in the market, with an increase interest of research [10, 29–34].

Studies carried out by Zhu and collaborators culminated in a foot sensor for measuring the pressure distribution while walking and shuffling. The system includes two insoles implemented with seven conductive polymer pressure sensors and respective electronic apparatus for an efficient data acquisition. The location of the pressure sensors was clinically certified by recording the walking pattern on a foot imprinter and then fixed in the heel, metatarsal and hallux areas. The pressure data was collected during trials of normal walking and shuffling, independently. Despite the interesting results presented, this system requires several electronic devices, such amplifiers, RAM's, microprocessors and other interface circuits that increase the complexity and weight of the arrangement [35, 36].

Wertsch *et al.* projected an insole sensor with seven piezo resistive sensors to evaluate pressure-time data. This insole was later remodeled by Hausdorff *et al.*, with the purpose of determining the temporal parameters of gait. Two force resistive sensors were placed under heel and toe to measure heel-strike and toe-off timing. Despite the goals achieved by the authors, there are some limitations in this system, related to the accuracy of discrimination of stance phase and correspondent portion of contact of heel and toe [37, 38].

A study by Kernozek *et al.* tested the feasibility of an in-shoe foot pressure system, based in an insole of capacitive sensors. In this study, the author determines the reliability coefficients of several parameters of plantar pressure, considering seven anatomical regions of greater interest, spread by heel, midfoot, metatarsal and toe [5].

Lawrence and Schmidt projected a wireless in-shoe force system intended for patients with impaired gait. The system consists of a pair of insoles capable of measuring the force applied in six areas of major interest, among those already mentioned in the studies above [39].

Yang and colleagues suggested a set of sensors dedicated to plantar pressure and knee joint angular movement. In detail, the plantar pressure sensors were designed with a base layer, coupled with a dome shape of styrene butadiene rubber, where two electrically conductive fibers were embedded. Four sensors were set in heel, middle lateral, metatarsal and toe areas. When pressed, the conductive fibers connect, turning into an "on" status. The sensors were tested in different walking routines and the information processed by a Bluetooth connected device, showing the path of the center of pressure (COP), in the insole [40].

De Rossi *et al.* produced an in-shoe device for pressure measurement, based in an array of sixty-four mechano-optoelectronic transducers, supported by on-board electronics to process the signal conditioning and wireless transmission. The transducer has a 12x12 mm base layer, where a LED and a photodiode are settled. Covering these optical components, there is an opaque silicone shell, which deforms when pressed, obstructing the free path of light, inducing a reduction in the photodiode input. The calibration of these sensors relates to the force applied by the output voltage of the photodiode, which can be analyzed by a computer or smartphone. Despite the vast number of sensors, the base electronics takes places in the own insole, preventing the measurement of pressure in the midfoot area [41-44].

Bamberg *et al.* presented a shoe-integrated wireless sensor system to determine the parameters that characterize gait pattern, using electronic devices as accelerometers, gyroscopes, polyvinylidene fluoride strips (PVDF), force sensitive resistors (FSR), bend and electric field sensors. These electronic sensors can display the orientation, velocity, force distribution, plantar and dorsi-flexion and heel-strike and toe-off timings. The FSRs were placed on four of the foot sole key points. The other sensors were placed along the longitudinal spindle of the insole. All the data collected by the insole sensors is transmitted by an antenna, integrated in the shoe [45].

Sazonov and collaborators conceptualized a wearable shoe-based device for rehabilitation of patients who experienced stroke scenarios, since in most cases, asynchronicity is reported. Similar to the Bamberg's system, mentioned above, it consisted of a pair of shoes with five pressure sensors incorporated in each insole, arranged in heel, metatarsal bones and toe. In addition, an accelerometer sensor was placed in the heel area, to add orientation and motion trajectory data. Like the abovementioned systems, each shoe is equipped with a microcontroller and a Bluetooth connection hardware, which transmits the collected information to posteriorly be displayed by a smartphone software [25, 46].

Another insole system using accelerometers, gyroscopes and force sensing resistors was tested by Querido *et al.* to ascertain the spatial-temporal gait parameters [47]. These parameters allied to the plantar pressure magnitude can be related with individual features of humans and can be perceived as a fingerprint, in personal identification. Feng and Yamakawa and their collaborators, developed two distinct systems of biometric identification, based in plantar pressure-time distribution, with a recognition rate of approximately 90% [33, 48, 49].

Anatomically, the walking routine is a complex process. As we know, the interaction between the skeletal structure and muscles with the floor involve not only the gravitational force induced by body weight on the sole of the feet, but also other-directional forces, such as shear stresses. The contribution of those forces is fundamental in normal gait, but it is also known that irregular magnitudes or repetitive stress can lead to irreversible foot pathologies. Therefore, clinical monitoring of plantar and shear pressure is fundamental to prevent ulceration of diabetic foot neuropathies [1, 2, 15, 50].

Marasović *et al.* studied the ground reaction forces in the gait pattern and evidenced the distinction between center of pressure and center of gravity. In his paper published in 2009, it is detailed the complete gait pattern in terms of vertical ground force and shear loads. The experiment was preformed using a force plate, equipped with conventional electronic transducers. It is shown the distinct stages of gait, as well as the direction of the forces, for a better understanding of the foot behavior while walking [10].

Years earlier, Tappin (1980) and Lord (1992) presented a method for shear stress measurement, with focus on the medical studies about diabetic plantar ulceration. The data acquired by the bi-directional shear transducers implemented under the five metatarsal bones' head – known to be the area of maximum load – demonstrated the several segments of shear stress and underlined its variation magnitude with the sensor location under foot [50, 51]. Also, for clinical shear stress measurement, Akhalaghi and Pepper introduced a bi-directional shear measurement system, developed at the University of Kent, England. Each insole, equipped with four biaxial transducers, is able to measure the longitudinal and transversal shear stress of heel, first and fifth metatarsals and toe (hallux) [52].

There are plenty other electronic sensing systems that are not contemplate in this chapter. Regardless of the fundamental contribution of these studies, there are inescapable disadvantages in the usage of electronic devices in everyday routine. A few studies intend to introduce the optical fibers in the biomechanics scope. The advantages of optical fibers may fill the gaps in the usage of electronic systems, such the dependency on electrical supply at the sensor point. The weightlessness, electromagnetic immunity and biocompatibility of optical fibers are suggestive features in human interacting sensors. Some contributions to the OFS applications in gait analysis are described below, featuring some of the devices previously reported.

Wang *et al.* formulated a sensing cell based in a macrobend sensor. An array of optical fibers composed by two layers of parallel fibers, perpendicularly between layers, operating

by power loss technique can measure pressure and shear stress. The design of the sensors is presented in the **Figure 1.2**.

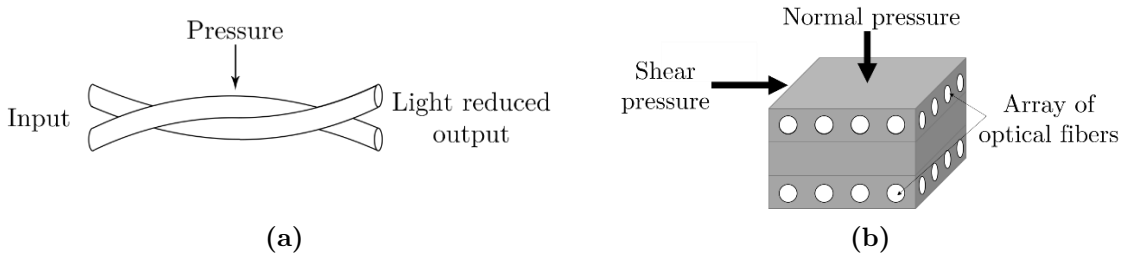

Figure 1.2 – **(a)** Schematic representation of the operating light loss principle. **(b)** Shear sensor design. *Adapted from Wang 2005.*

Based in this solution, topographic force maps can be generated by output intensity data, to evaluate the spatial prolongation of the pressure and shear stress applied. Despite of the results, this prototype exhibits several drawbacks when integrated in a wearable sensor system. The size and number of optical fibers required in each cell are some of its limitations [15].

Also, the fiber Bragg gratings' working principle has been extensively studied in the recent years. As we know, its response to strain and temperature is largely appreciated in the optical sensors field. Based in this principle, Kanellos *et al.* designed a two-dimensional pressure sensor using one optical fiber with multiple FBGs embedded in a polymeric sheet, with 2.5 mm of thickness. In this experiment, 4 FBGs were used in a sensing pad (2 per 2). The wavelength shift and reflected optical power losses were monitored when a force was applied, resulting in a subsequent FBG elongation. This system revealed a sensitivity of 10% optical power loss per 10 kPa of pressure and a spatial resolution of 1 cm^2. The multiplexing ability and reduced thickness of the sensor enables its implantation in diverse environments, suited for several biomedical applications [53].

Koulaxouzidis *et al.* developed a pressure and shear stress sensor, using three FBGs embedded in an elastomer cube, placed in different directions. Using a similar configuration, Zhang and his collaborators developed, in 2013, a pressure and shear stress sensor, based in two FBGs, embedded in a polydimethyl-siloxane matrix. One FBG is placed horizontally, to measure the vertical force, while the other FBG is placed in the elastomer matrix in a quasi-diagonal orientation, as show in the **Figure 1.3**.

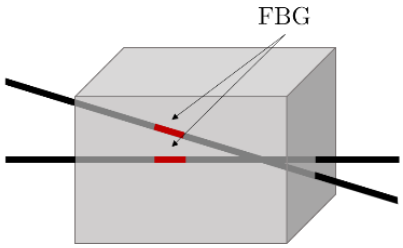

Figure 1.3 – Schematic representation of the sensing cell.

The authors also conducted a simulation by the finite elements method to evaluate the strain along the fiber with and without gaskets and its interaction in the fiber-matrix bounding. The performance test was made using four gaskets, revealing a pressure sensitivity of 0.8 pm/Pa and shear stress sensitivity of 1.3 pm/Pa [54, 55].

1.4. Goal and motivation

Despite the wide stock of electronic plantar pressure sensors, they still present several limitations in their working process and implementation procedure, requiring electrical supply in the sensing point and heavy shielding of the electronic components. The size and weight are aspects that compromise the versatility and adaptability of these electronic systems. However, the scientific evolution – of optical fibers, in particular – suggest that better sensing configurations can be conceived and implemented in systems to enhance the life's quality of world citizens [56].

Optical fibers are seen as a reliable replacement of the conventional sensing technology and their development have been widely enlarged in the last decades. The reduced size, humidity resistance and ability to operate at long distance from the power source, appoint optical fibers as a huge competitor to mature technologies. Also, the biocompatibility, multiplexing ability and flexibility to attach to complex geometry make optical fibers especially suited for health monitoring sensing [32, 56–59]

Based in the abovementioned features and considering the scientific progress already made in the health monitoring – in particular, in gait analysis – and the gaps this technology still has, it is proposed in this project, a biaxial optical fiber sensor, for simultaneous plantar and shear pressures measurement. Based in the strain dependence behavior of the FBGs, several sensor configurations were tested and upgraded, for plantar and shear pressures monitoring, culminating in the integration of those sensors in wearable insoles. The insoles prove to be a non-evasive solution for real-time gait monitoring to be used in e-Health

platforms, prepared for daily medical use, acting as an important tool to aid the prevention and diagnosis of foot related diseases.

1.5. Synopsis

This dissertation is divided into five chapters. This first chapter contains a brief introduction to foot anatomy, gait pattern dynamics and the common pathologies that can influence the normal gait. Also, it is presented the state of art regarding the scientific advances and the existing technology in the areas of gait analysis and plantar pressures sensors. The chapter ends with the presentation of the main objectives and the motivation for the development of this scientific work.

The second chapter consists of a theoretical description of the optical fibers work principle and main features. Then, an introduction to fiber Bragg grating, its production and advantageous application as sensors are presented.

The third chapter introduces the design and testing of different sensing cells configurations, for monitoring of plantar and shear pressures. In this study, it is evaluated the suitability of the materials used for future integration in a shoe insole. In that sense, the material's physical properties were studied, as well as the overall operation mode of the sensing cell.

In the fourth chapter it is presented the insoles design, comprising the integration of five sensing cells in key points of analysis. The results of the tests in laboratory environment are also presented in this chapter, as well as the possible e-Health architecture in which the developed insole can act as an enabler.

The fifth, and last chapter, presents a conclusion on the work here developed and a perspective on future work.

Chapter 2

2. Optical fiber sensors

The invention of lasers in the 1960's, provided optical fibers technology a remarkable evolution, sharping their usage for numerous purposes, from telecommunications to sensing applications [30, 56, 60]. The automation of processes in the modern industry and new technological trends like the Internet of Things (IoT) came to bring vital importance to sensor devices. The photosensitivity phenomenon demonstrated in the research conducted by Hill *et al.* (1978) and the possibility of writing Bragg gratings in a fiber core, unlocked the opportunity of using optical fibers as intrinsic sensing elements. In this chapter the standard optical fiber concept is introduced and, in more detail, the fiber Bragg grating's writing process and working principle as a sensing component is presented [60–64].

2.1. Working principle

The optical fiber is an optical waveguide that consists of a dielectric structure, almost transparent to the operational wavelength. The cylindrical central layer – entitled as *core* – is surrounded by a concentric layer – the *cladding* – with a lower refractive index. The cladding role in the optical fiber is to ensure a uniform refractive index wrapping the optical fiber, so the light reflected in the bound core-cladding sustains its uniform propagation in the core of the fiber. However, any contamination of the cladding constitution may change the course of light in the fiber core. Also, most fibers, have a plastic coating for physical protection of the inner layers of the fiber [60, 65, 66].

The optical signal inserted in the optical fiber is concentrated in the core and can be transmitted from hundreds of kilometers due to the total internal reflection, a phenomenon sustained by the difference between the refractive indexes of core and cladding. **Figure 2.1** presents a schematic representation of this transmission phenomenon. The difference of

refractive indexes can be abrupt – in step profile fibers – or gradual, called graded profile optical fibers. To ensure that light remains inside the core, the internal reflection must obey Snell's Law for incident angles lower than the critical angle ϕ_c [59, 65, 66].

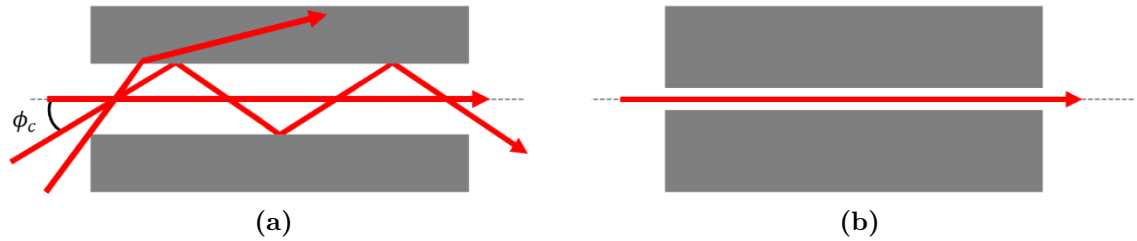

Figure 2.1 – **(a)** Multimode and **(b)** single-mode waveguides. $\phi_c = sin^{-1}\left(\frac{n_2}{n_1}\right)$, where n_1 and n_2 are the core and cladding refractive index, respectively.

Nowadays, optical fibers are widely used in telecommunications – largely for long-distance communications. Optical fiber signal's transmission depends on two basic parameters: the attenuation and the bandwidth. Also, absorption by the fiber material and scattering of the light beam out the core induces power loss of the light signal. Thus, attenuation is especially important because it defines the distance limit of transmission without the need for repeaters. Since their first development, continuous progress was made to reduce the power loss of the transmitted light, converging in a loss rate of 0.2 dB per kilometer, in the 1550 nm wavelength region. There are other low attenuation windows used in optical fiber communications, located in the range around 850 and 1300nm. The first one (850nm) present higher losses than the other two low attenuation windows, and so, it is suited for short-medium distance transmission [65–67].

The light in the fiber, as an electromagnetic wave, can be propagated in a series of possible modes. In fact, this introduce a common problem in optical fibers communications, the intermodal dispersion, where the arriving time of the multiple modes is different. In order to minimize this effect, it is used single-mode fibers which have a very small core diameter in relation to multimode fibers (typically 5 μm *to* 10 μm, compared to multimode fibers that can reach core diameters of 200 μm) and operate with light wavelengths close to 1500 nm. Mostly composed by silica, these single mode fibers are widely used, transmitting only a single guided mode, with a reduced modal dispersion [9, 60, 61, 65, 66].

2.2. Fiber Bragg gratings

The optical fiber photosensitivity represents the amount of variation of the refractive index of the core, that can be changed by ultraviolet (UV) laser emission and is a key feature for the Bragg grating production. The discovery of this characteristic in the optical fibers is a

remarkable technological advance in the area of optical sensors, as well as a reasonable commercial alternative, mainly in the academic and experimental environment.

Fiber Bragg gratings (FBGs) are periodic structures which can be photo-inscribed in the core of the optical fiber, along their longitudinal axis, by permanently changing its refractive index. There are several types of Bragg structures which are differentiated by the angle and spacing of the grating planes. The blazed Bragg grating, the chirped Bragg grating and the Bragg reflector are some examples, among other novel configurations constantly studied. The Bragg reflector is the most common structure holding the same spacing between the grating planes, perpendicular to the fiber axis (**Figure 2.2**) [58, 64, 68].

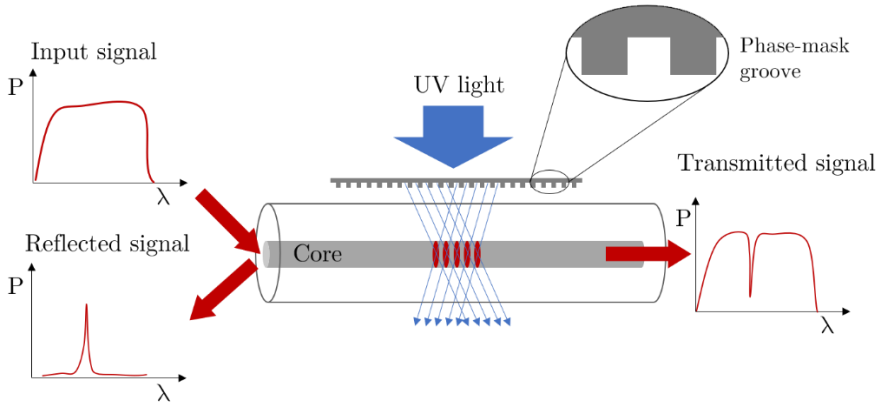

Figure 2.2 – Schematic representation of the phase-mask writing technique and FBG response signals.

Beyond the multiple methods for grating writing, the phase-mask technique gets detailed in this chapter, for its efficiency and recurrent use in the experimental tasks of this work. This method requires a diffractive element – the phase-mask – which is a one-dimension surface-relief, transparent to UV light. The phase mask technique greatly reduces the complexity of the fabrication process of FBGs, being a feasible, stable and reproducible method for this type of gratings. When the phase mask is aligned with the fiber core and once the UV beam (244-248 nm) is launched, it creates an interference pattern, which modulates the refractive index of the optical fiber core [57, 64, 69, 70].

The Bragg grating condition implies the conservation of energy and momentum. Energy conservation is guaranteed when the frequency of incident and reflected radiation is the same. To assure the same for momentum, the wavevector of the diffracted radiation, $\boldsymbol{k_f}$, equals the wavevector of the incident wave, $\boldsymbol{k_i}$, in addition to the grating wavevector, $\boldsymbol{K}$ **(1)**.

$$\boldsymbol{k_i} + \boldsymbol{K} = \boldsymbol{k_f} \ . \qquad (1)$$

The magnitude of the grating wavevector is $\frac{2\pi}{\Lambda}$. The incident and diffracted wavevector have the same magnitude, but opposite direction. Hence, equation **(2)** becomes

$$2\left(\frac{2\pi n_{eff}}{\lambda_B}\right) = \frac{2\pi}{\Lambda} \, . \qquad (2)$$

The center wavelength of the reflection band (Bragg wavelength, λ_B) is related to the effective modal refractive index and the periodic refractive index modulation, as described in equation **(3)**, and it is known as the first order Bragg condition

$$\lambda_B = 2n_{eff}\Lambda \, . \qquad (3)$$

The reflectivity in the periodic perturbation of the refractive index, Λ, can be understood as Fresnel's reflection phenomenon, acting as a mirror for wavelengths that assures the Bragg condition. For a normal incidence, the reflection coefficient, R_F, is given by

$$R_F = \left(\frac{n_1 - n_2}{n_1 + n_2}\right)^2, \qquad (4)$$

where n_1 and n_2 are two different refractive indexes of the surfaces involved in the reflection [71, 72]. Beside this dependency, the reflected signal of FBGs has a direct relation with strain and temperature. The sensitivity to such parameters is the major characteristic that allows optical fibers Bragg gratings to operate as intrinsic sensors. The change in the effective refractive index, as in the periodic spacing between the grating planes, induces a shift in the Bragg wavelength, described by equation **(5)** [31, 58, 64, 73–75].

$$\Delta\lambda_B = 2\left(\Lambda\frac{dn}{dl} + n\frac{d\Lambda}{dl}\right)\Delta l + 2\left(\Lambda\frac{dn}{dT} + n\frac{d\Lambda}{dT}\right)\Delta T \qquad (5)$$

The increase of the fiber's mechanical strain or temperature, in the FBG region, induces a positive shift in the Bragg wavelength. Since FBGs have residual hysteresis, the opposite behavior is also observed [15, 76]. Despite the high sensitivity of the FBGs, this binary dependence introduces several drawbacks in the sensors operation, when just one of the contributions is required for monitoring certain parameters. To discriminate the contributions of strain or temperature, some variations of the sensor scheme can be implemented, like strain-free FBGs as a reference for the device temperature. There are also other alternative demodulation techniques presented in the literature, such as first and second diffraction wavelength of Bragg gratings and superimposed FBGs to measure strain and temperature [8, 30].

Chapter 3

3. Sensing cells

As described in section **2.2.**, FGBs dependency on strain and temperature allows its application as sensors devices that operate in response to these physical parameters. Furthermore, when incorporated in certain configuration, FBG can also operate as sensors for other variables that directly depend of those above-mentioned parameters, like pressure, shear stress, acceleration and even chemical parameters [30, 77]. In this chapter, the design and implementation of a compact optical fiber sensor based on two multiplexed fiber Bragg gratings for the simultaneous measurement of plantar and shear pressures is described.

3.1. Sensing cells design

To manage the foot's plantar and shear pressures analysis, the sensor's development started by the design of four sensing cell configurations, able to be multiplexed and networked for future integration in a shoe insole. The configurations are described in the **Table 1**, named as A, B, C and D. All configurations comprise two multiplexed FBGs. Also, it was used the same materials in their fabrication, although with different layouts and configurations, taking advantage of their intrinsic characteristics under compression.

The ideal sensing cell should be able to discriminate plantar and shear pressures in the same exact point. However, due to the limitations of the prototype it was adopted a two-FBGs solution (2 mm long), written apart with an approximate distance of 9 mm. The sensing cells were made on a 3D printed polymer base (polylactic acid – PLA), with two cavities spatially delimited. The FBGs, were then inserted in the cell, placing one FBG in each cavity. The cavities were completed/filled with different materials, namely cork and a thermo-setting epoxy resin (Liquid Lens Advanced, United Kingdom™). Those different materials, composing each cavity, induce different sensitivities in the FBGs, regarding their

response to plantar and shear pressures, which is a crucial factor for the following demodulation of the optical signal, described in the next section of this chapter.

Table 1 – Four sensing cell configurations

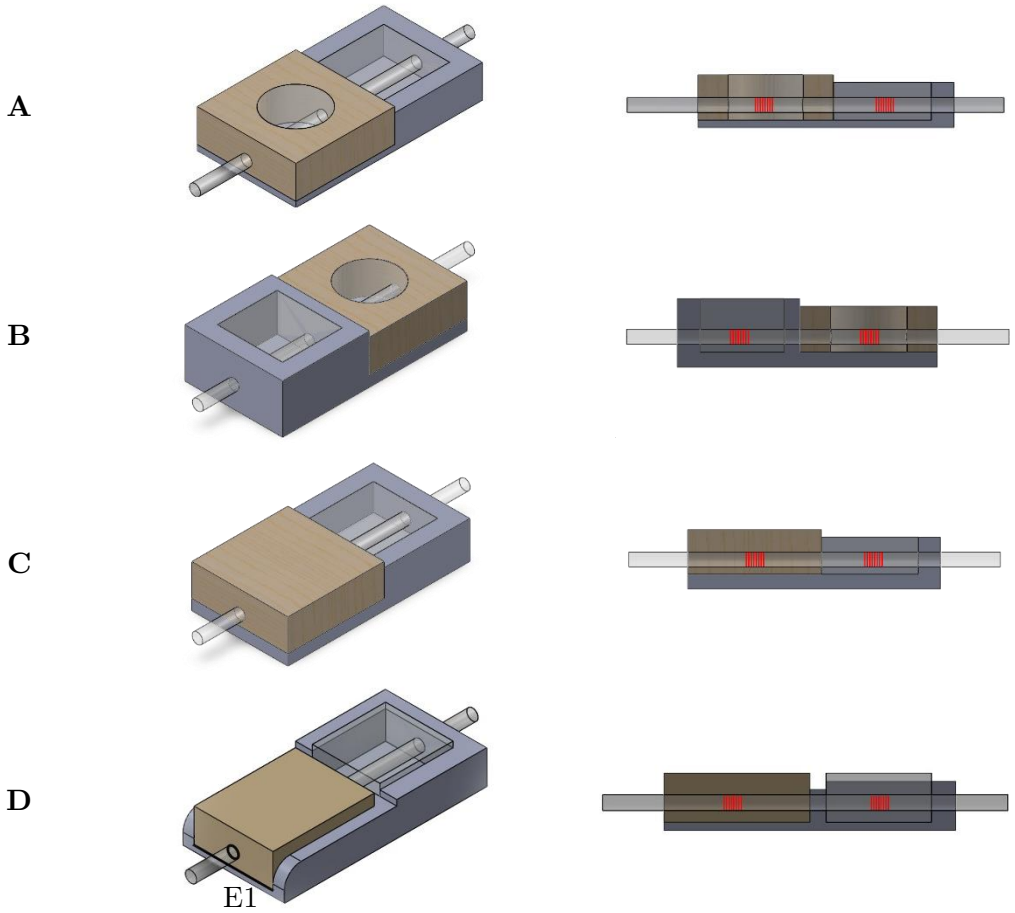

The red stripes over the fiber indicates the FBGs position. The optical fibers are not to scale. Black lines represent the glued edges.

In configuration A, the cavity 1 is isolated by a square piece of granulate cork (9x9x3 mm) with a 2.5 mm radius hole in the center. This cavity was selected to have a stronger response to normal pressure measurement, since the cork provides mechanical isolation from lateral forces applied in the sensing cell, due to the almost zero Poisson coefficient [78]. The cavity 2, designed for an enhanced sensitivity to horizontal pressure measurement, is surrounded by polymer walls with 1.5 mm thick and 2.5 mm height, and slightly lower than cork wall. The optical fiber crosses both cavities, with each FBG adjusted in their center. The cavities are then filled with epoxy resin, to provide protection and ensure the necessary robustness to the sensing cell. The optical fiber is embedded in the resin inside the cavities,

without any other attachment point. The pressure applied to the epoxy resin in cavities 1 and 2 is also transmitted to the FBG embedded therein [73].

Configuration B has the same components as the version A, with only the switching of the cavities design. In this version, the cavity 1 preserves the polymer wall height and thickness and cavity 2 is isolated with a square piece of cork. Both cavities were filled with the same epoxy resin. The polymer walls are higher than the cavity 2 and between them, it was added another polymeric wall with 1 mm thickness to ensure a better structural stability to the sensing cell and to prevent the lateral deformation of the epoxy resin, when horizontal pressure is applied.

The configuration C was built over the same polymeric base, but the piece of cork that isolates the cavity 1 does not contain the hole in the center. In this configuration, the optical fiber passes through the cork and remains completely isolated from the other components. The cavity 2 has the same size and materials as version A.

The fourth configuration, named as D, was idealized after the first calibration tests of the three configurations described above, attempting to overcome the limitations verified (that will be explored in the following sections). Over the polymeric base already used in the other configurations and using the design of configuration C as the starting point, there were added two PLA walls in cavity 1, among which was placed a piece of cork (9x6x3 mm). Since no resin was applied to the piece of cork, the fiber was fixed with cyanoacrylate glue on the exposed face of the cork, that is also fixed in the edge E1 (**Table 1**). The cavity 2 is separated from cavity 1 by a 1 mm thick PLA wall, which was designed to have an enhanced response to plantar pressure.

All sensing cells were then covered by a thin layer of epoxy resin (approximately 2 mm thick) to provide robustness to the overall cell and to protect the FBGs. The stiffness of the epoxy resin does not prevent the normal operation of the sensing cell, since its deformation propagates along the material, ultimately deforming the contained FBGs.

3.2. Materials and pressure range

To test the operability of the materials used in the production of the cells and to implement the respective computer simulations, tensile and repeatability tests were carried out on PLA polymer, epoxy resin and cork. For tensile testing, there were used three samples of each material (80x21 mm), with rectangular cross section and gauge length of 21 mm. For each material, three samples were tested, under the same conditions. The average results are

presented in the **Figure 3.1**. The tests were performed using a Shimadzu™ AGS-X tensile test machine.

Based in Hooke's law, the stress (σ) applied to a material can be related with the consequent strain (ε), under a proportional constant E, termed as Young's Modulus. This relation is valid for materials that exhibit a linear elastic behavior, wherein Young's modulus is defined as the slope of the linear portion of the stress-strain diagram [79, 80]. The Poisson's ratio is calculated as the quotient of the variations of longitudinal length and width of the sample [79].

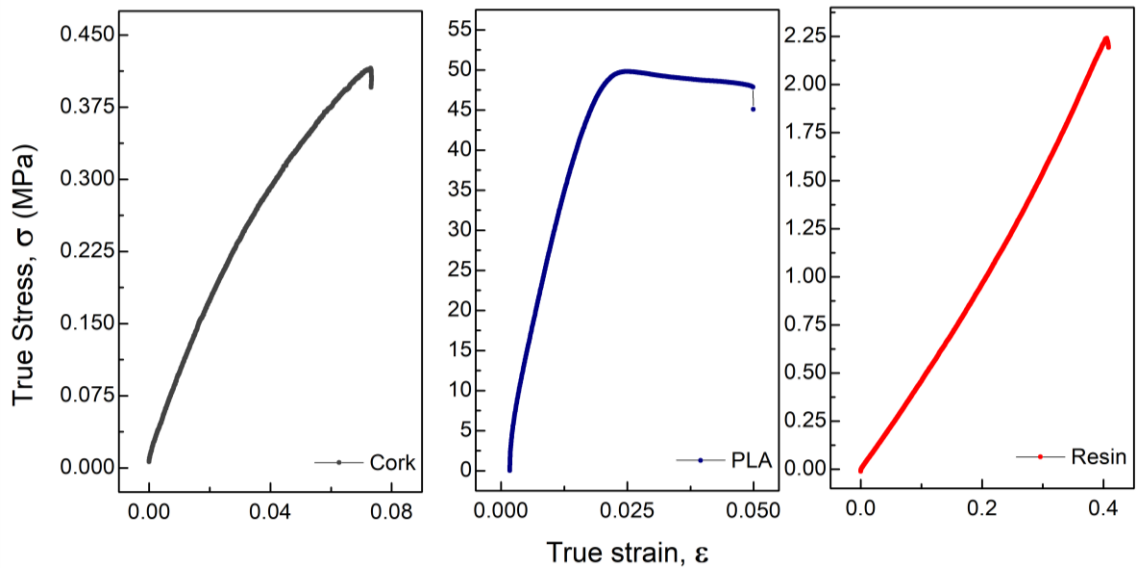

Figure 3.1 – Tensile tests average results for cork, PLA polymer and epoxy resin.

As it can be seen, these materials reveal a non-linear elastic behavior (more evident in resin and cork stress-strain curves). In literature, there are two methods to measure the Young's modulus, described as tangent and secant modulus. These two methods serve as approximations to the linear elastic behavior and the Young's modulus is stated by the slope of the secant or tangent lines to stress-strain curves. In computer-aid analysis it is commonly used the tangent modulus approximation, adopted in this analysis [79, 80].

Since the results obtained for the epoxy resin do not match the typical parameters for this material, they were discarded. The deviation of results is due to air bubbles that are trapped in the material, weakening those areas and promoting the premature break of the resin test pieces. Thus, Young's modulus values and Poisson's coefficient were adopted in the material library of an Ansys® 19 simulation software.

The results are presented in **Table 2**, with the correspondent Poisson's ratio.

Table 2 – Young's Modulus determined by tangent modulus and Poisson's ratio of the three materials (r^2: 0.9957 – 0.9995).

Material	Young's Modulus (*MPa*)	Poisson's ratio
PLA	3004.836	0.235
Epoxy resin*	3780	0.35
Cork	8.791	0.052

**from Ansys 19 Materials' library*

In the repeatability loading tests, the physical stability of the materials under repeated pressure loads was tested. The aim was to check the behavior of the different materials of the sensing cell, simulating the repeated use of the insoles. For that purpose, ten consecutive compression trials of 200±3 N (≈1,3072 MPa) were performed, over square samples (9x9x3 mm) of the same abovementioned materials (**Figure 3.2**). These tests were performed in a Shimadzu™ AGS-5KND tensile test machine.

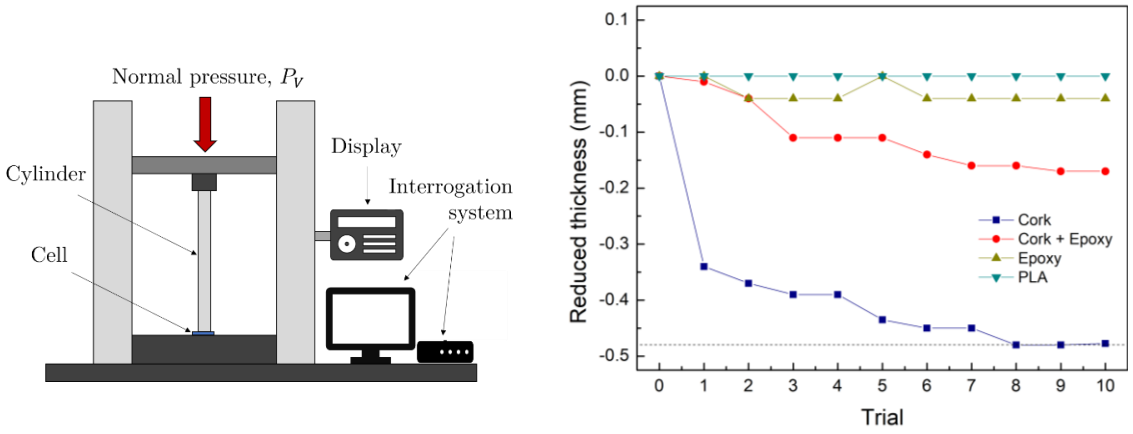

Figure 3.2 – **(a)** Scheme of the experimental setup. **(b)** Repeatability tests results.

The cork samples revealed a trend of initial thickness reduction, when applied repeated loads of approximately 200±3 N (**Figure 3.2 b**). Although it is a natural material, in this case the cork used in the construction of the sensing cells came from composite cork sheets, formed by a granulate of this material. Under repeated compression, the granulate becomes more compact, reducing its initial thickness to decreasingly constant values, with an observed minimum of about 0.5 mm. However, in sensing cells A and B, this effect is not determinant to sensor's operability, since the cork is embedded in epoxy resin, revealing a residual thickness reduction (0.17 mm after ten compression trials). PLA polymer and epoxy resin samples preserved their initial thickness during the trials, even at higher pressures (>500 N), which ensures good structural resistance to the insole.

Following up the loading tests, it was also carried out a compression limit test to understand the pressure's threshold that can be applied to the sensing cell without breaking the FBGs embedded in it. A sensing cell (configuration A) was subjected to normal force, in increments of 20 N, up to the rupture of one of the fiber Bragg gratings of the cell, which happened for a load of 240 N. In **Figure 3.3** is presented the resistance test of sensing cell A, showing the wavelength shift curve of FBGs 1 and 2 until the optical fiber rupture, between them.

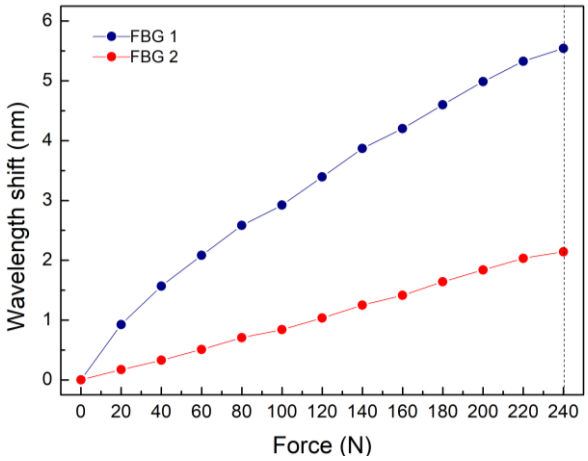

Figure 3.3 – Resistance test of sensing cell A. *Dotted line indicates the force limit.*

Since the materials used in the other configurations is the same, it is expected that they would present similar behavior. Considering the sensor area (1.44×10^{-4} m^2), the rupture limits obtained, imply a pressure limit of 1.67 MPa. Comparing the pressure limit of the optical fiber sensor with previously published works, it is verified that the pressure limit obtained is above the typical peak pressure values (PPP), obtained in trials while standing, and as presented in **Figure 3.4**.

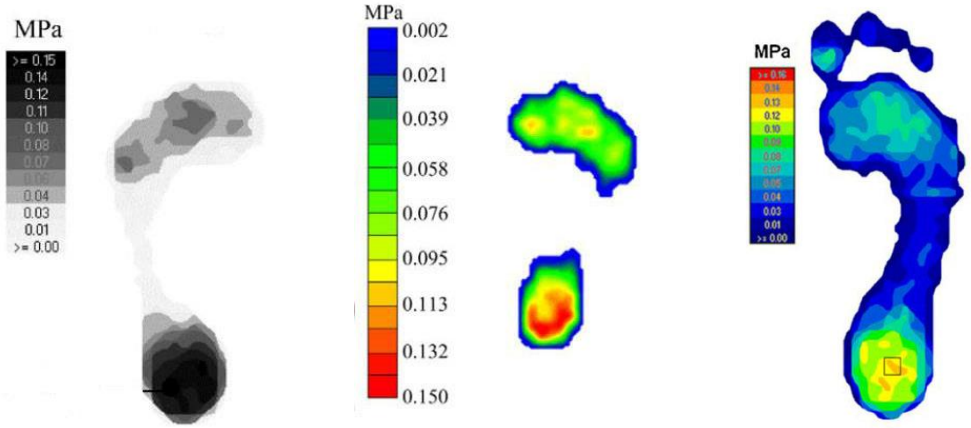

Cheung *et al.*, 2005 [81] (PPP=0.17 MPa)

Tao *et al.*, 2009 [82] (PPP=0.15 MPa)

Cheng *et al.*, 2010 [83] (PPP=0.13 MPa)

Figure 3.4 – Pressure maps presented in previous reports.

In addition, the peak plantar pressure and peak maximum shear stress (PMSS) values – while walking – are also presented in previous reports. **Table 3** summarizes some of plantar and shear pressure ranges, presented in previous studies, using different sensing technologies.

Table 3 – Pressure range presented in previous studies

Author	Sensing site	PPP (kPa)	PMSS (kPa)
Lebar *et al.* (1996) [84]	1st and 5th metatarsals, hallux and posterior heel.	5.4 – 43.5	6.7 – 51.4
Lord and Hosein (2000) [85]	1st to 4th metatarsals and heel	187 – 273	(39.4 – 72.7)
Hosein and Lord (2000) [86]	1st to 4th metatarsals and heel	152 – 228	31.0 – 86.5
Perry *et al.* (2002) [87]	Toe and metatarsals*	80 – 189	(18 – 33)
Zou *et al.* (2006) [88]	Forefoot and rearfoot	272 – 371	(66.6 – 78.7)
Mueller *et al.* (2008) [89]	Forefoot and rearfoot*	325 – 739 (387 - 988)	70 – 170 (93 – 230)
Lott *et al.* (2008) [90]	Forefoot	328 (414)	70 (90)

*trials performed with barefoot

() - refer to subjects with *diabetes mellitus* or other associated pathologies.

The plantar and shear pressures' values may differ due to different subject's aspects, such as weight, age and pathologic history. Also, a variation can be attributed to sensor's calibration, size, resolution or other intrinsic features [84, 91]. However, considering the order of magnitude of the results, the sensors cells' design can be considered validated. After the materials characterization, the sensing cells were subjected to an individual calibration, detailed in the section **3.3**.

Also, hysteresis tests were performed on sensing cell A, using the same setup of the resistance test. The figure below shows the results of the wavelength shift under compression and decompression of both FBGs (loads up to 100 N).

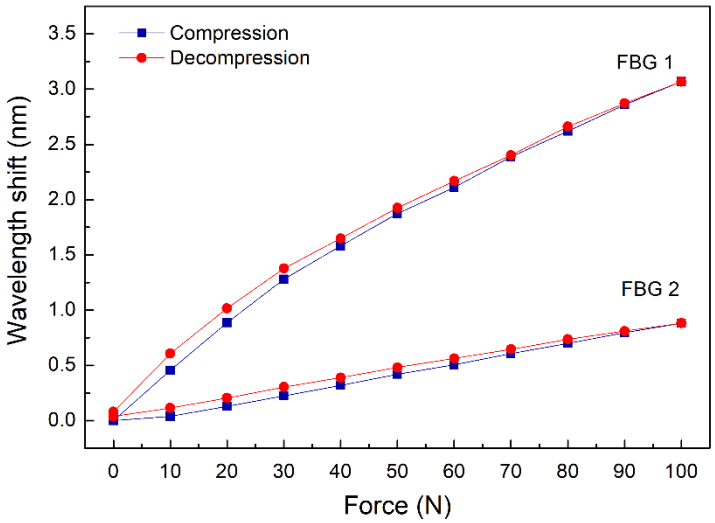

Figure 3.5 – Resistance test of sensing cell A. *Dotted line indicates the force limit.*

It is verified that each FBG follow a similar behavior in compression and decompression, proving that the hysteresis affecting the FBGs signal is residual.

3.3. Calibration and Performance Testing

Since the feedback of the FBGs is encoded in Bragg wavelength shift, $\Delta\lambda_B$, the sensors require a normal pressure (P_V) and horizontal pressure (P_S) calibration, to discriminate the dependence of this parameter with strain variation, $\Delta\varepsilon$, in the FBG **(6)**

$$\Delta\lambda = \mathrm{K}_{\varepsilon}\Delta\varepsilon \ , \qquad (6)$$

where K_{ε} is the sensitivity to strain variation. For the plantar pressure and shear pressure calibration, it was determined the response of both FBGs to normal pressure and horizontal pressure, respectively.

The sensing cells were tested and calibrated using a 3-axial electronic force sensor, composed by one biaxial (MBA40, Futek, Irvine, CA, USA) and one uniaxial (TPP-3/75, Transdutec, Barcelona, Spain) units (**Figure 3.6**).

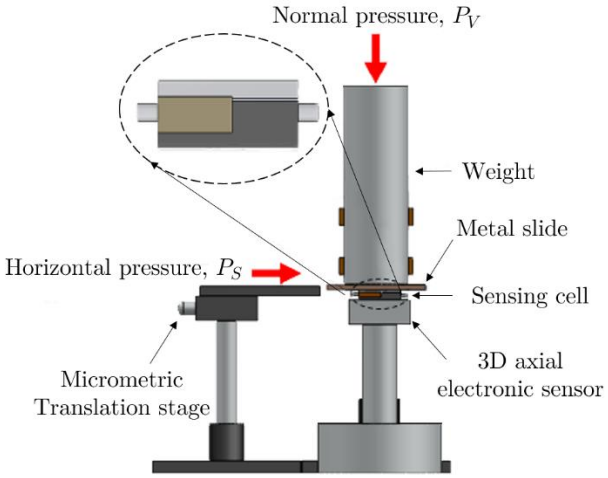

Figure 3.6 – Scheme of the experimental setup for the calibration and testing of the sensing cell.

Due to logistic procedures, the plantar pressure calibration of sensing cells B and C was performed using a Shimadzu™ tensile test machine (**Figure 3.2 a**). The reflected optical signal of the FBGs was acquired by an I-MON 512 USB (Ibsen, Farum, Denmark) interrogation system, with a resolution of 5 pm.

Figure 3.7 (a) shows the typical response of the electronic force sensor and **Figure 3.7 (b)** shows the FBG sensing cells signal to the same applied normal force, with an evident increase of the force applied in the normal direction. The respective FBG response, is marked by an increase of the wavelength shift, due to the elongation of the optical fiber under normal pressure.

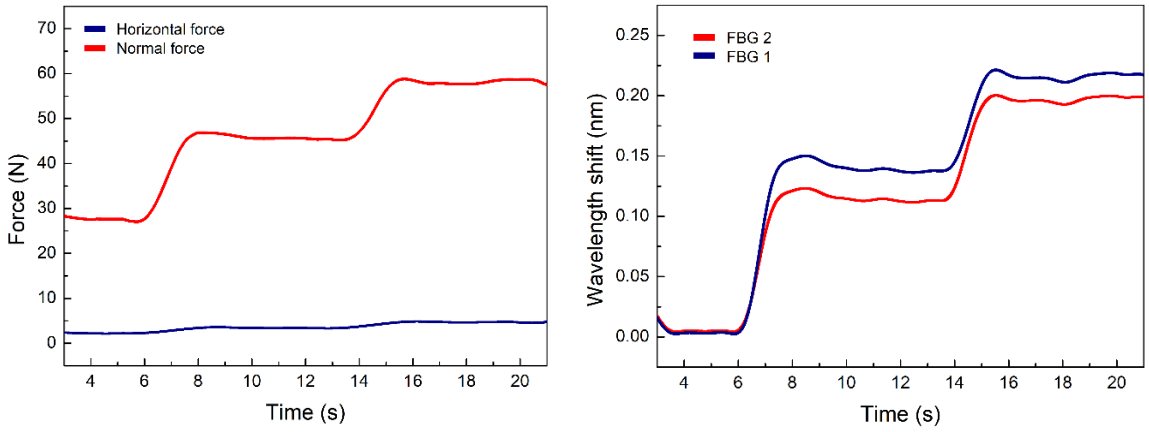

(a) **(b)**

Figure 3.7 – Data acquired by **(a)** the 3-axial electronic sensor and by **(b)** the optical fiber system, under normal force.

The results presented in **Figure 3.8** are related to horizontal force applied to the sensing cell, by sliding the metal piece placed between the sensing cell and the weight.

Figure 3.8 (a) shows the response of the electronic sensor while **(b)** corresponds to Bragg wavelength shifts registered for the sensing cell FBGs. It should be noted that the sliding of the metal piece was driven by cyclic movements of a translational stage, hence, the obtained results present such periodic oscillatory pattern.

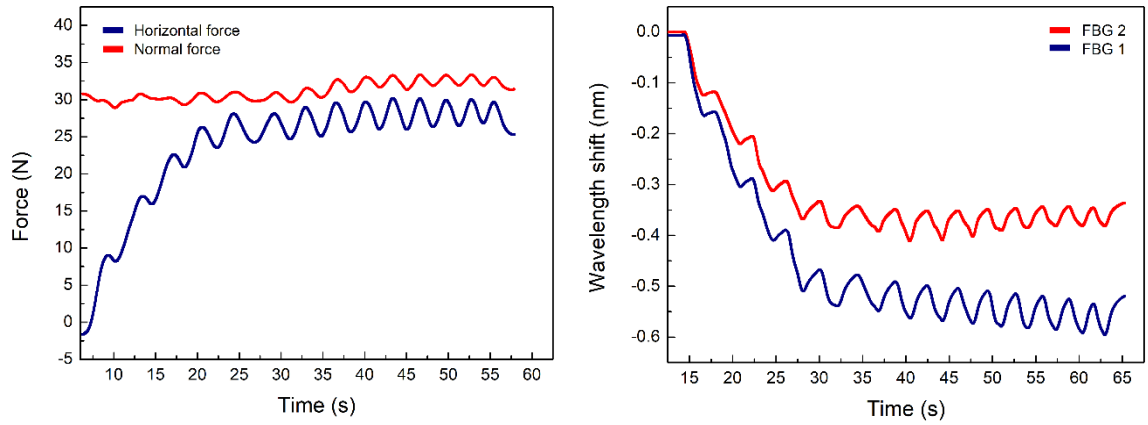

(a) **(b)**

Figure 3.8 - Data acquired by **(a)** the 3-axial electronic sensor and by **(b)** the optical fiber system, under horizontal force.

From this initial test, it became clear that both FBG sensors respond to the two forces applied: normal and shear force. Therefore, it is necessary to calibrate the sensing cell to normal and horizontal pressures, independently. The calibration of the FBGs is shown in next sections, with the wavelength shift as a function of pressure.

3.3.1. Sensing cell A

Sensing cell A calibration was performed in the 3-axial electronic sensor, according to the experimental set-up shown in **Figure 3.6**. The several levels of normal pressure were applied with the aid of a mass metal cylinder (≈ 3 Kg), with a diameter of 28 mm, adequate to cover the whole area of the sensing cell.

For the horizontal pressure calibration, a metal slide was placed between the cylinder and the sensing cell to slide over the surface of the cell. Horizontal pressure's calibration test was performed using the translation stage (**Figure 3.6**). The movement correspondent to a complete turn of the micrometric screw ($\approx 360°$), increases the horizontal pressure in the cell's surface.

The electronic and optical raw signals were smoothed by applying fast Fourier transform (FFT, 100 points) and Savitsky-Golay (100 points) filters, respectively. Also, force values were converted to pressure (in kPa), to standardize the unit system used in the comparison of the several theoretical and experimentally obtained data. **Figure 3.9** represents the Bragg

wavelength shift as function of the normal **(a)** and horizontal **(b)** pressures applied, registered by FBG 1 and FBG 2.

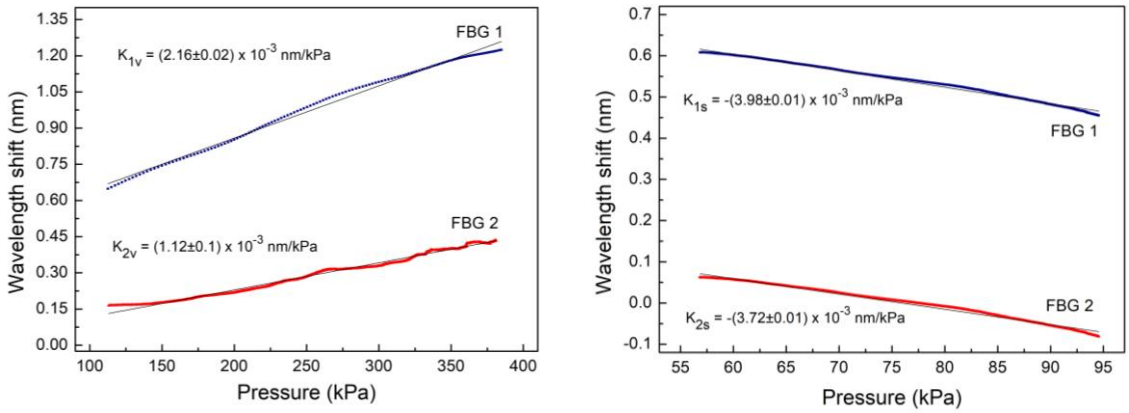

(a) **(b)**

Figure 3.9 – Calibration data of FBG1 and FBG2, under **(a)** normal pressure and **(b)** horizontal pressure. (Sensing cell **A**).

By linearization, the calibration constants, corresponding to the sensitivities of FBG 1 and 2 as a function of normal (K_{1V} (FBG 1), K_{2V} (FBG 2)) and horizontal pressure (K_{1S} (FBG 1), K_{2S} (FBG 2)), are:

Table 4 – Sensitivities of FBG 1 and 2, for sensing cell **A**.

$\mathbf{K_{1V}}$ ($\times 10^{-3}$ nm/kPa)	$\mathbf{K_{1S}}$ ($\times 10^{-3}$ nm/kPa)	$\mathbf{K_{2V}}$ ($\times 10^{-3}$ nm/kPa)	$\mathbf{K_{2S}}$ ($\times 10^{-3}$ nm/kPa)
2.16 ± 0.02	-3.98 ± 0.01	1.12 ± 0.01	-3.72 ± 0.01

3.3.2. Sensing cell B

The sensing cell was fixed to the base of the electromechanical test machine and remained under constant compression of a 25.00 ± 0.01 mm steel cylinder. An increase of 10 ± 3 N load were applied per trial (≈ 65.4 kPa) up to approximately 650 kPa. The horizontal pressure calibration was performed using the 3-axial electronic sensor, with the same method abovementioned. The obtained results for both calibrations processes are represented in **Figure 3.10**.

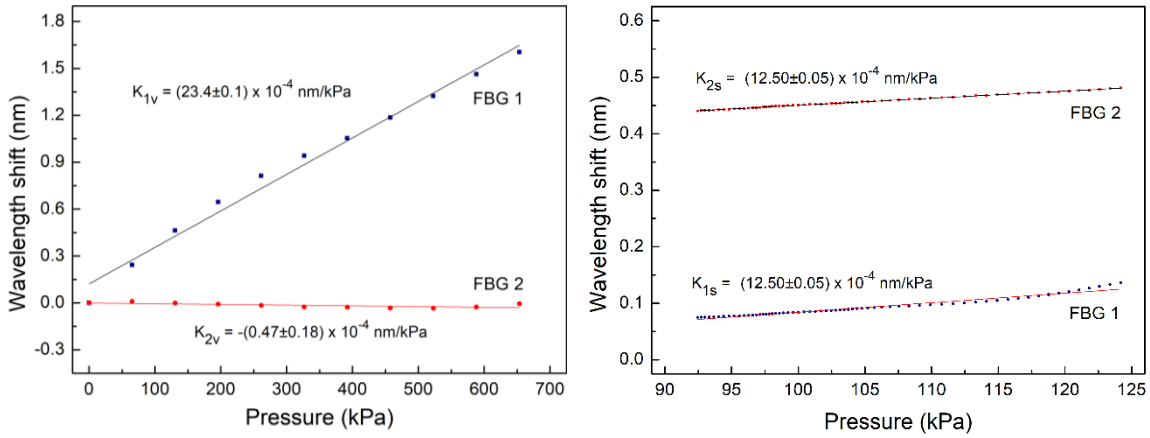

Figure 3.10 – Calibration data of FBG1 and FBG2, under **(a)** normal pressure and **(b)** horizontal pressure. (Sensing cell B)

As it can be seen, the sensitivity of the FBG 2, $K_{2V,}$ under normal pressure is relatively small when compared with the sensitivity of the FBG 1, K_{1V}. A reasonable explanation is that the epoxy resin may had exceed the limits of the cavity, forming a higher gap between the cavities and therefore, leaving the FBG 2 less sensitive under normal pressure. Also, the polymer wall separating the cavities of the sensing cell may have influenced these results. In fact, the epoxy resin in cavity 1 is surrounded by walls of hard polymer, which when under compression, will induce the epoxy resin to expand through the hole where the optical fiber crosses the cavities, compressing the FBG 2. This effect may have the added influence of cancel out the FBG 2 deformation. From the results of the linear fitting, the sensitivities were determined as presented in the table below.

Table 5 – Sensitivities of FBG 1 and 2, for sensing cell **B**.

$\mathbf{K_{1V}}$ ($\times 10^{-4}$ nm/kPa)	$\mathbf{K_{1S}}$ ($\times 10^{-4}$ nm/kPa)	$\mathbf{K_{2V}}$ ($\times 10^{-4}$ nm/kPa)	$\mathbf{K_{2S}}$ ($\times 10^{-4}$ nm/kPa)
23.4 ± 0.1	12.50 ± 0.05	-0.47 ± 0.18	12.50 ± 0.05

3.3.3. Sensing cell C

After applying the same calibration methodology of sensing cell B, it was foreseen that this configuration does not meet the requirements for a quality plantar pressure measurement. Surely it is clear in the **Figure 3.11** that this configuration does not show a prominent sensitivity to normal pressure, as the response of FBG 1 is considerably weaker than FBG 2, when under normal pressure.

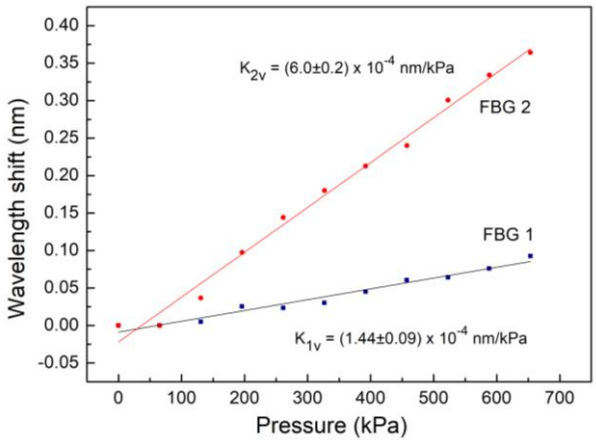

Figure 3.11 – Calibration data of FBG1 and FBG2, under normal pressure. (Sensing cell C)

The normal pressure sensitivities obtained for FBG 1 and FBG 2 are presented in **Table 6**.

Table 6 – Sensitivities of FBG 1 and 2, for sensing cell **C**.

$\mathbf{K_{1V}}$ ($\times 10^{-4}$ nm/kPa)	$\mathbf{K_{1S}}$	$\mathbf{K_{2V}}$ ($\times 10^{-4}$ nm/kPa)	$\mathbf{K_{2S}}$
1.44 ± 0.09	$--$	6.0 ± 0.2	$--$

The sensitivity to normal pressure of both FBGs, indicates that this solution would not be ideal for the application in mind. Therefore, this solution was not further pursued, and horizontal pressure calibration was not made. However, by observing the results of this sensor cell, the initial idea was reformulated. Given the poor response of cork when a normal pressure is applied to its surface, the new design developed as already detailed in section **3.1**, culminating in the configuration D.

3.3.4. Sensing cell D

In this configuration, the orientation of the sensor cells was switched, in relation to the other sensing cells. The working principle of this cell is based on the fact that the piece of cork (without resin) in cavity 1 should be more responsive to horizontal pressure than to normal pressure – due to the compression margin it still exhibits – allowing future demodulation of wavelength shifts into the respective pressures. **Figure 3.12** shows the linear dependence of each FBG to normal and horizontal pressures.

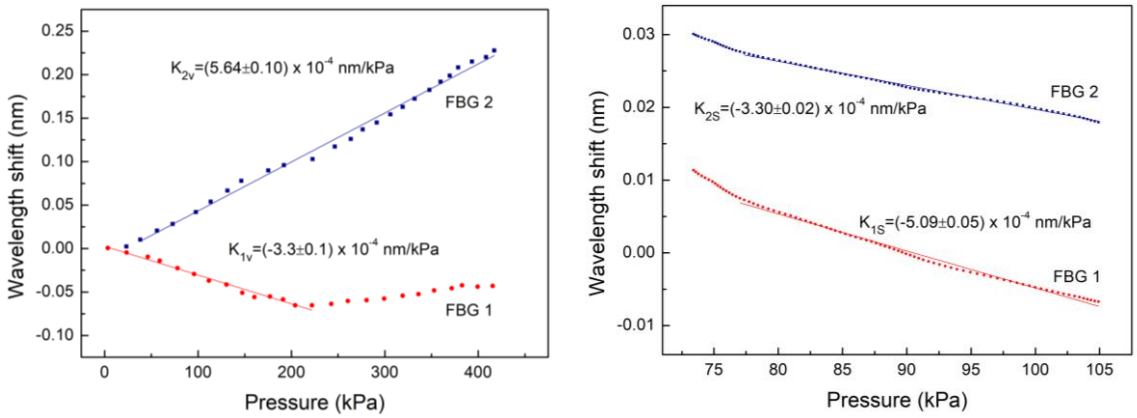

(a) **(b)**

Figure 3.12 – Wavelength shift of FBG 1 and 2, under **(a)** normal pressure and **(b)** horizontal pressure.

The sensitivities obtained for FBG 1 and FBG 2 were as follows, in **Table 7**:

Table 7 – Sensitivities of FBG 1 and 2, for sensing cell D.

$\mathbf{K_{1V}}$ ($\times 10^{-4}$ nm/kPa)	$\mathbf{K_{1S}}$ ($\times 10^{-4}$ nm/kPa)	$\mathbf{K_{2V}}$ ($\times 10^{-4}$ nm/kPa)	$\mathbf{K_{2S}}$ ($\times 10^{-4}$ nm/kPa)
-3.3 ± 0.1	-5.09 ± 0.05	5.64 ± 0.10	-3.30 ± 0.02

The calibration results of this sensing cell lead to some additional considerations. As can be seen in **Figure 3.12**, the FBG 1 has a dual behavior under normal pressure. The FBG 1 compresses up to about 220 kPa, point after which the FBG reveals a constant behavior. One indicator to explain the relaxation of the FBG 1 is the distention of the piece of cork to higher pressures (> 220 kPa). For a better understanding of this behavior, it was used a computer simulation, where the stress map and behavior of the cell's materials under normal pressure (500 kPa) can be observed.

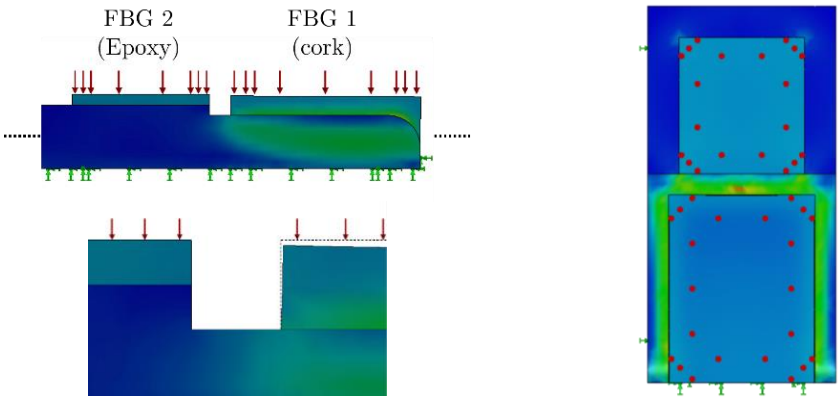

Figure 3.13 - Sensing cell's stress (von Mises) simulation. *Dotted line indicates the initial position of the cork piece. Red arrows (or dots) represent the pressure vectors.*

Note that for simplification of the simulation, the optical fiber and the epoxy cover layer were ignored. Pressure was equally applied over the surfaces of epoxy and cork.

In the calibration of sensing cell C, it was found poor response of the cork to normal pressure. Considering cell D, it seems that the FBG 1 signal is obtained not by compression of the cork, but by feedback of the pressure applied on the cavity 2 (epoxy resin), until a certain limit. The epoxy resin, when compressed, occupies the hole in the wall that bounds the two cavities. In fact, in **Figure 3.13,** it is possible to see a point of maximum tension at the center of the polymer wall. Since the optical fiber inside the cork is loose, fixed only in the front face, this behavior forces the FBG's compression, up to a limit observed at 220 kPa.

Despite the dependence of the FBG response on temperature, no thermal calibration was performed on the sensor cells. The reason for this decision is based on two assumptions: for fast-analyzes (<1 minute), the heat transfer between the human body and the sensor is not sufficient to distort the results of the pressure to which it is subject. On the other hand, in the case of prolonged use, it is assumed that sensors acquire the constant temperature of the human body. Once stabled, the temperature ceases to be a distorting factor of the FBG signal.

3.4. Simultaneous P_V and P_S loadings

After calibrations, the sensing cells were tested for simultaneous normal (P_V) and horizontal (P_S) pressures monitoring.

The test was performed on the sensing cell, fixed to the 3-axial electronic sensor, under normal and horizontal pressure, simultaneously. There were performed trials of increasing normal pressure, complemented by the induction of horizontal (shear) pressure, using the micrometric screw. The responses of both FBGs to the two stimuli were recorded by the electronic sensor and interrogation system software. The data acquired by the two FBGs of each sensing cell can be related to the pressure applied through a two-equation system **(7)** [64, 92, 93]

$$\begin{bmatrix} P_V \\ P_S \end{bmatrix} = \frac{1}{d} \begin{bmatrix} K_{2S} & -K_{1S} \\ -K_{2V} & K_{1V} \end{bmatrix} \begin{bmatrix} \Delta\lambda_{B1} \\ \Delta\lambda_{B2} \end{bmatrix}, \qquad (7)$$

where $\Delta\lambda_{B1}$ and $\Delta\lambda_{B2}$ are the Bragg wavelength shift of FBGs 1 and 2, respectively, and d is the matrix determinant. This mathematical method was used in the test data of cells A and D, detailed in the following sections.

3.4.1. Sensing cell A performance test

Following the procedure described above, it was simulated the pressure pattern during normal walking on the sensing cell A. Using the calibration constants determined in section **3.3.1**, the system becomes

$$\begin{bmatrix} P_V \\ P_S \end{bmatrix} = \frac{1}{-3.58 \times 10^{-6}} \times \begin{bmatrix} -3.72 \times 10^{-3} & 3.98 \times 10^{-3} \\ -1.12 \times 10^{-3} & 2.16 \times 10^{-3} \end{bmatrix} \begin{bmatrix} \Delta\lambda_{B1} \\ \Delta\lambda_{B2} \end{bmatrix}. \qquad (8)$$

Figure 3.14 shows the results of the performance test of sensing cell A. It is clear the horizontal pressure variations (red line), induced in the cell surface, under increasing normal pressure (blue line). The raw data of the optical sensors **(a)** was introduced in equation **(8)** to calculate the aftermath demodulated signal of FBG 1 and 2, presented in **(b)**. The data acquired by the electronic 3 axial sensor **(c)** serve as reference, to verify the quality of the demodulated signals of the optical sensors. In fact, signal from plot **(c)** is quite similar to the electronic reference, being concordant with the expected result of this test.

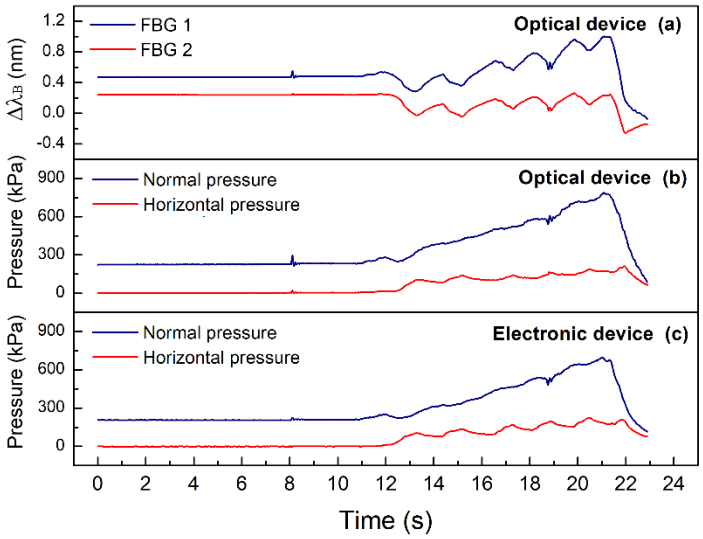

Figure 3.14 – Performance test of sensing cell A.

In more detail, the curves of normal and horizontal pressure of the optical device are compared with the reference signal. **Figure 3.15** shows normalized curves of both normal and shear pressures.

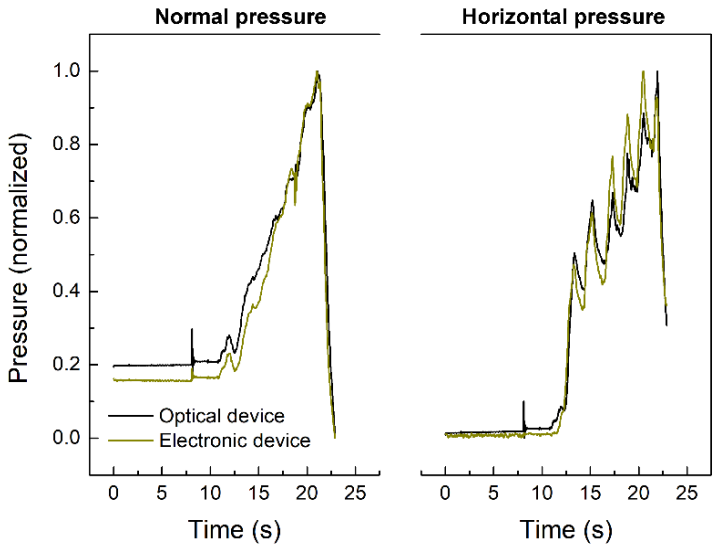

Figure 3.15 – Normalized curves for normal and horizontal pressures (sensing cell A). $RMSE_V$=0.0535; $RMSE_S$=0.0487.

The results of this sensor cell enable its introduction in shoe insoles for gait analysis, as a non-invasively solution, compatible with normal locomotion functions. Its test on an integrated multi-sensor system for foot pressure monitoring is detailed in the next chapter.

3.4.2. Sensing cell D performance test

The performance test was repeated for sensing cell D. For the results' evaluation, only pressure values up to 220 kPa were considered in the operational test proceedings. In fact, by observation it was concluded that for values above this threshold, the FBG's response ceases to be concordant with the reference values obtained by the electronic sensor. The results of the performance test are presented in **Figure 3.16**.

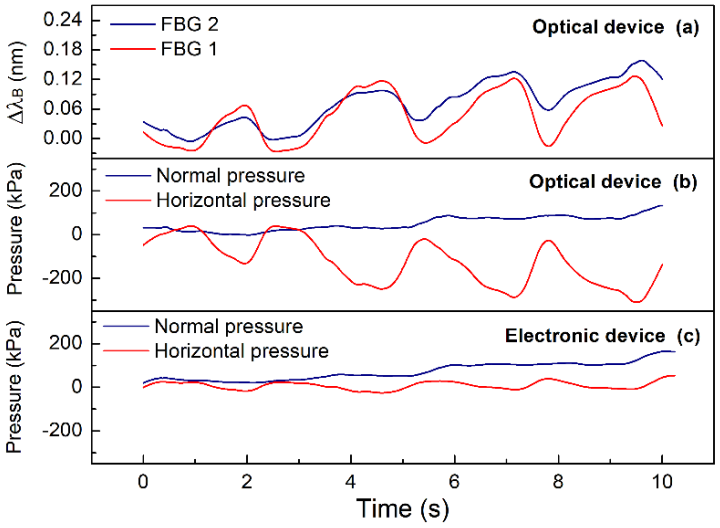

Figure 3.16 – Performance test of sensing cell D.

Firstly, the optical device's normal pressure values seem to agree with the normal pressure values measured by the electronic sensor. In detail, **Figure 3.17** shows comparison between the values of both sensors and the normalized curves.

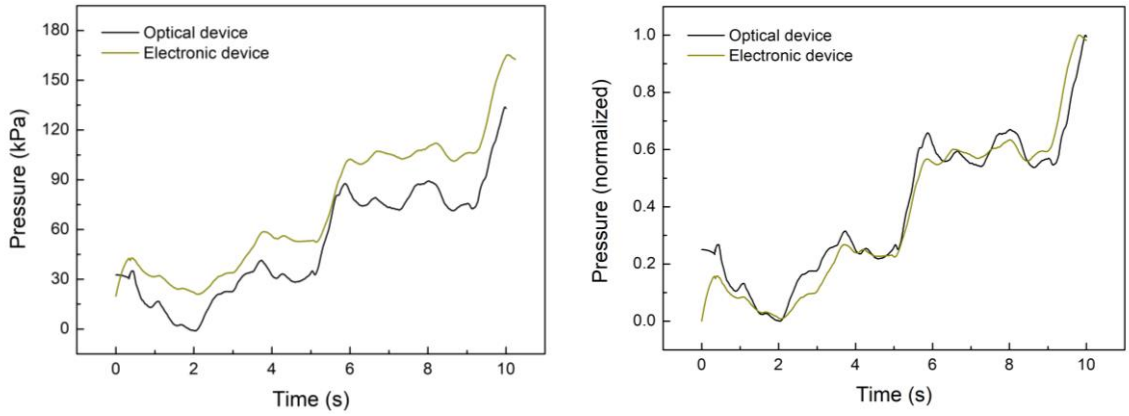

Figure 3.17 – **(a)** Comparison of normal pressure curves, measured in both sensors and **(b)** the normalized curves for normal pressures. $RMSE_V$=0.0625.

However, the shear pressure values obtained in the optical sensor reveal very different magnitudes from those observed in the electronic sensor. In addition, the optical signal seems to follow a decreasing trend, probably influenced by the normal pressure component. In fact, as observed in the calibration, a possible dependence of the FBG 1 signal when compressing the FBG 2 is expected, so that is verified in the performance tests.

To verify this dependence, we studied a window of values from where the cell is without influence of the normal pressure. The results are shown in **Figure 3.18**.

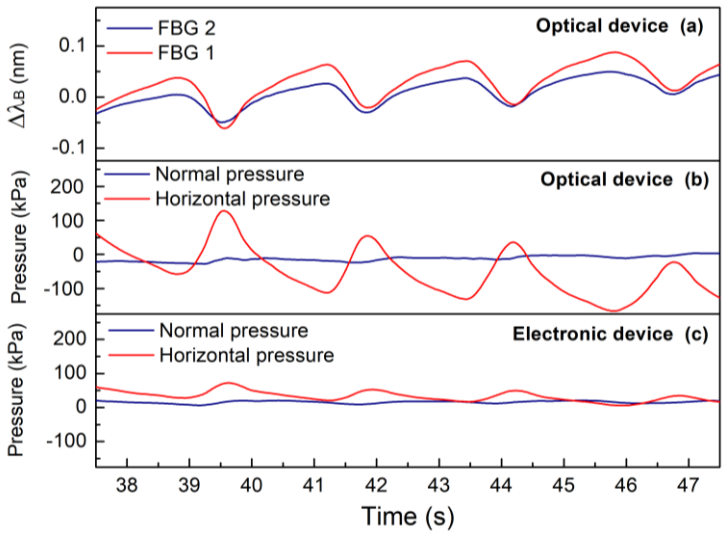

Figure 3.18 - Performance test of sensing cell D, without normal pressure applied.

In fact, the descending trend is less evident now, which confirms the dependence of the signal of FBG 1 with the compression of FBG 2. However, the difference of magnitudes prevails, which possibly indicates a problem in the calibration. The fact that the cork used is a granular material, allowing some compression, may have incremented the effect just noticed. The cork, when compressed by normal pressure, becomes more compact around the fiber. Thus, the optical fiber that once had room to move inside the piece of cork, now finds more friction and, therefore, more feedback of the horizontal pressure applied in the cork. In conclusion, this reasoning concludes that this configuration is not adequate for monitoring shear pressure, since it does not contemplate the structural alterations of cork when under normal pressure.

Chapter 4

4. Gait Analysis

In this chapter is presented the insoles with the sensor cells implemented, as well as the results of simultaneous plantar and shear pressure monitoring. It is detailed the several components of the insoles, as well as their assembly process and testing. Finally, it follows the interpretation of the performance tests, with some comments about the obtained sensors signal quality.

4.1. Insole design and testing

Considering previously published studies and interpreting its results of the plantar pressure map, five sensing cells were manufactured in each insole, placed in points of greater interest to monitor. According to the reported maps of plantar pressure, the areas under greater pressure are the heel and the metatarsals' heads (**Figure 3.4**). These are areas where shear pressure is equally prominent, with the addition of the hallux region.

4.1.1. Epoxy insoles

Figure 4.1 (a) is a schematic representation of the epoxy insoles – in this case with sensing cells A – where is presented the main direction of plantar and shear pressure vectors. Note that the shear pressure vector is bi-directional, since in a normal gait pattern, the anterior-posterior force is observed in the beginning of the walking routine when heel strikes the floor, then starting the pushing movement, with the posterior-anterior force [10]. In the notation of **Figure 4.1 (b)**, P-points are those associated with plantar pressure sensors and S-points are related to shear pressure measurements.

The insole consists of a 1 mm thick PLA printed layer, which the sensors cells lie, aligned with heel, first and third metatarsals, midfoot and toe positions. Over the layer 1, it was placed a second layer of epoxy resin (3 mm), marked with the optical fiber guides (layer 2).

The optical fiber containing 10 multiplexed FBGs (with a length of 2 mm each) was positioned through the fiber guides, connecting all the sensing cells, so each cell houses two FBGs. Finally, the insole is covered with another layer of epoxy, with 2 mm thickness, to protect the sensors, ensure structural robustness, facilitate the cleaning and even soften the surface of contact with the human foot.

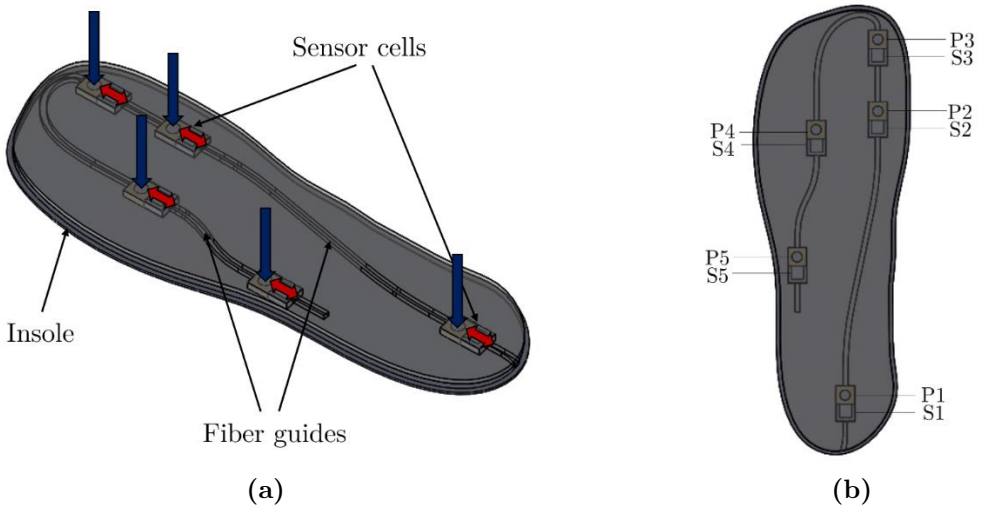

Figure 4.1 - **(a)** Scheme of a sensing insole with cells A and **(b)** sensing cells position.

The FBGs were written in a GF1 photosensitive optical fiber (Thorlabs®), by phase-mask technique, using a UV Bragg Star™ Industrial-LN pulsed KrF excimer laser, operating at 248 nm. The applied pulse energy has 5 mJ with a frequency of 500 Hz.

The optical fiber is loose throughout the path within the fiber guide, being held only by the epoxy resin, in the sensing cells' cavities. The developed system allows the simultaneous monitoring of plantar and shear pressures throughout the foots' sole, with sensors responding to the plantar and shear pressures, and thus, to control the gait pattern of the patient.

To complete the insole production process, all the sensing cells used in the insole were individually calibrated, since the sensitivity of the FBG's can change from cell to cell. The cell calibration process followed the same method described in section **3.3**, to obtain the sensitivity of FBGs for normal pressure (K_{1V} and K_{2V}) and for shear pressure (K_{1S} and K_{2S}). Since all the FBGs were written in a single optical fiber – which passes through all the sensor cells – all the optical power peaks, corresponding to the reflected Bragg wavelengths, are observed on the same spectrum. **Figure 4.2** shows the optical spectra, under normal loading on points P5/S5 of the insole, for four stages of loading.

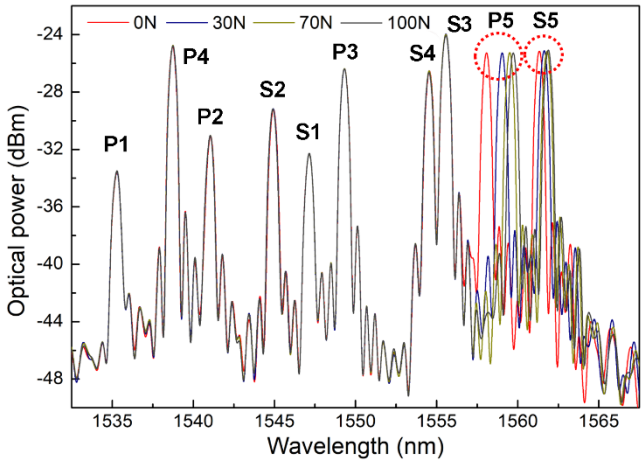

Figure 4.2 – Optical spectra obtained under normal pressure.

As predicted, sensor P5 has a prominent sensitivity to normal pressure in relation to S5, while all the other sensors remain unchanged. This isolation characteristic is a necessary condition for the proper operation of the sensing insole, so the pressure applied on a specific point does not affect the response of neighboring sensors of the insole.

After the calibration procedure, the sensing insole was installed in a shoe for a dynamic monitoring testing. The test consisted in monitoring the normal walking of a healthy subject (female, 45 kgs, barefoot), by recording the Bragg wavelength shift values, $\Delta\lambda_B$, of all FBGs, for a few steps, on a flat floor. **Figure 4.3** presents the results of the five sensing cells, during a 3 seconds walk. The signal from P1 was ignored due to interrogation system's malfunction, causing extensive gaps in the recorded values.

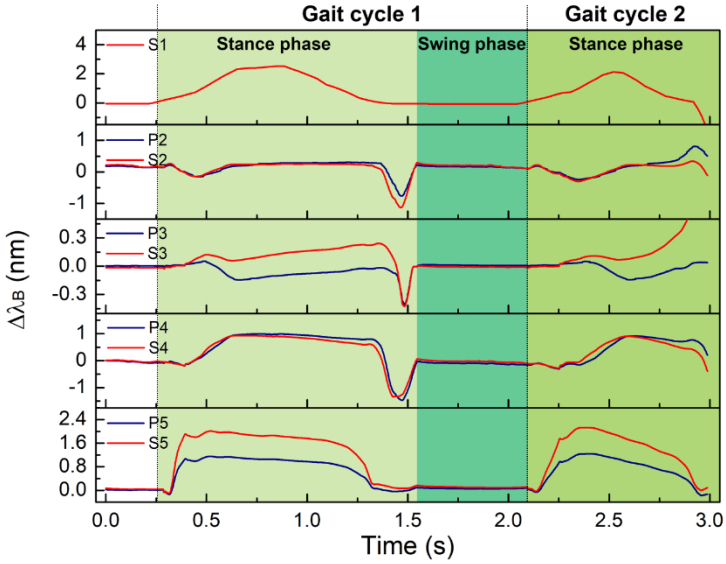

Figure 4.3 – Wavelength shift, $\Delta\lambda_B$, during stance and swing phase, registered for each FBG of the five sensing cells.

The results presented correspond to the FBGs optical signal directly observed in the interrogation system. Since the FBGs of each sensing cell respond to both pressure components (before demodulation), the start and end timings of each step of the gait are easily verifiable. Thus, after the first wavelength shift, the stance phase begins, which lasts until the stabilization of the Bragg wavelength shift around the initial value, marking the beginning the swing phase (**Figure 4.3**).

With the sensitivities obtained in the calibration (present in **Table 8**), it was proceeded the demodulation of the wavelength shifts into plantar and shear pressure values.

Table 8 – Insole's sensing cells sensitivities.

Sensing cell	$\mathbf{K_{1V}}$ ($\times 10^{-3}$ nm/kPa)	$\mathbf{K_{1S}}$ ($\times 10^{-3}$ nm/kPa)	$\mathbf{K_{2V}}$ ($\times 10^{-3}$ nm/kPa)	$\mathbf{K_{2S}}$ ($\times 10^{-3}$ nm/kPa)
2	3.9 ± 0.2	-1.1 ± 0.2	1.24 ± 0.08	-4.9 ± 0.5
3	7.1 ± 0.2	-2.28 ± 0.03	2.29 ± 0.07	-1.77 ± 0.02
4	2.2 ± 0.2	-35.15 ± 0.04	0.24 ± 0.04	-16.91 ± 0.07
5	2.9 ± 0.3	-0.68 ± 0.07	0.82 ± 0.08	-1.29 ± 0.02

The result of the demodulation of the plantar and shear pressures (using equation **(8)**) is shown in **Figure 4.4**. The shear pressure's signal of the mid-foot (sensor cell 5) was ignored.

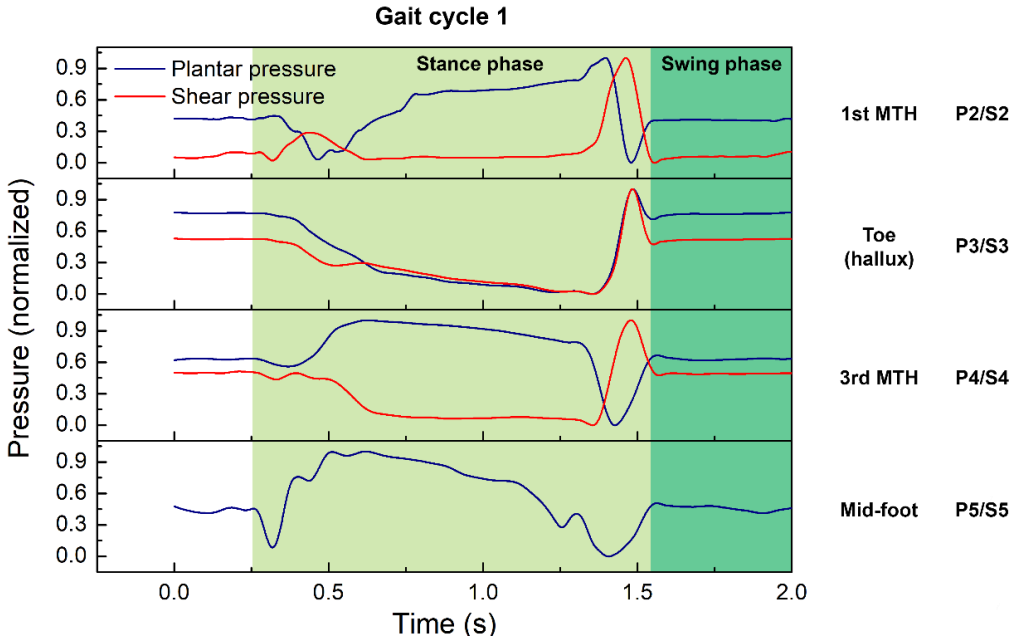

Figure 4.4 – Normalized plantar and shear pressures during stance and swing phase. *MTH=metatarsal.*

Figure 4.5 is an expanded section of figure above, for the first metatarsal area (sensing cell 2), for the gait cycle 1.

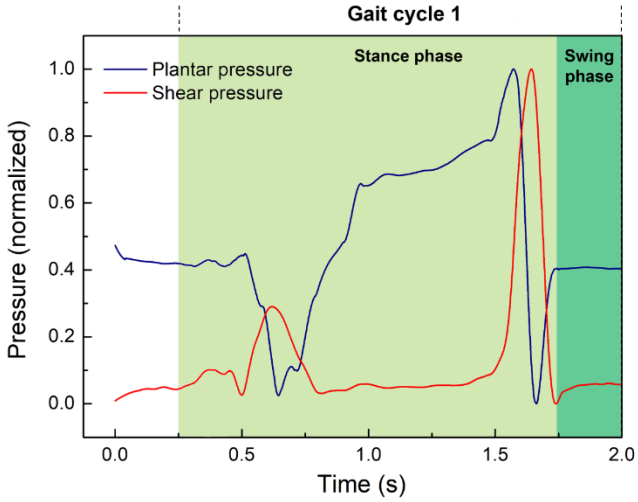

Figure 4.5 – Wavelength shift during stance and swing phase, for the first metatarsal.

Once this sensing cell was placed underneath the first metatarsal region, the first peak of shear pressure is related to the beginning of the foot-flat moment. It is also evident an intense peak of shear pressure in the toe, first and third metatarsals, at the end of the stance phase (**Figure 4.4**). This characteristic is associated with the force applied in the movement of the body, at the moments of heel-off and toe-off.

The metatarsal region is reported as the area with the highest magnitude of shear pressure. **Figure 4.6** shows the shear pressure curves for the first and third metatarsals during a gait cycle.

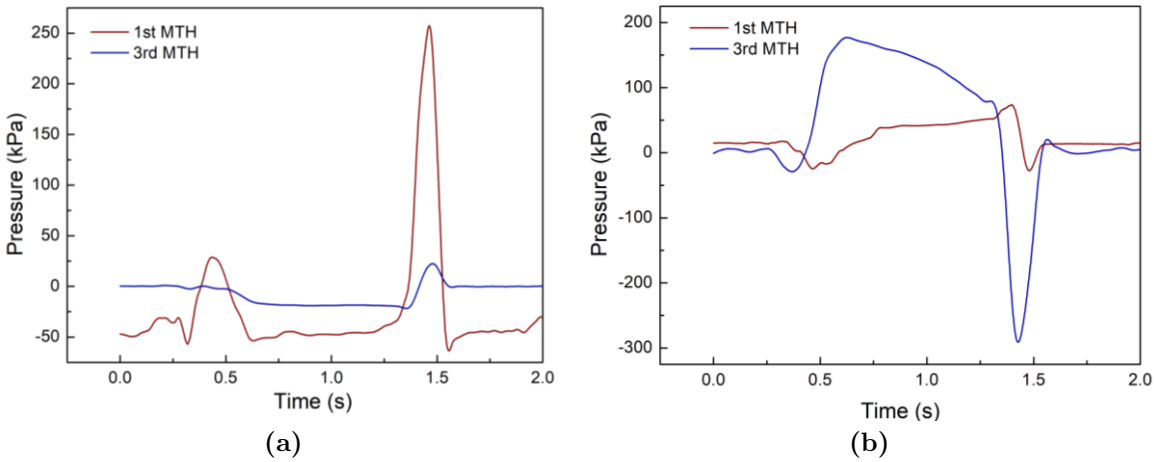

Figure 4.6 – **(a)** Shear pressure and **(b)** plantar pressure curves for first and third metatarsals (stance phase)

Again, a peak of shear is evident in both curves. The sensing cell 2 (first metatarsal) also records an intensity peaks at the beginning of the stance phase (already mentioned), which limit a lower pressure valley in between, possibly attenuated by the contribution of plantar pressure. In fact, although the successful demodulation of the two pressure components, the interference effects between FBGs signals are still not totally negligible.

The plantar pressure curves show a pressure band, with a peak of maximum pressure at the different timings of the stance phase, which is consistent with other plantar pressure monitoring studies, using other methodologies [35, 45, 49].

Finally, at point 3 (toe), it is clear that the wavelength shift of FBG 2 exceeds the shift of FBG 1 (**Figure 4.4**). In fact, it induced a misrepresentation of plantar pressure values, leading to unrealistic contribution to shear pressures. From literature we know that shear pressure values are usually lower than plantar pressure (**Table 3)**. Based on the insole design, it can be assumed that the results may have been influenced by the curvature made by the fiber around the sensing cell 3.

Chapter 5

5. Conclusion and future work

This work allowed to study pressure sensors based on FBGs and their application in a multiplexed system for monitoring simultaneous plantar and shear pressures. From all the idealized sensing cells - and within those that were tested - the satisfactory results of the sensing cells A are highlighted and its implementation in an insole was successful. The proposed cell architecture proved to be an efficient solution, making use of the intrinsic advantages of optical fibers, which make this type of device a feasible alternative to conventional technologies available in the market.

However, some limitations still prevail in the designed optical sensor, which may motivate its optimization in the future. Thus, the difficulties observed in the manufacture of these sensors, as well as a description of their failures in the operation, are presented below.

Materials

The cork reveals a low Poisson's ratio and its introduction in the sensor cells A was based on the removal of possible contributions of lateral forces exerted in the sensing cell, privileging the signal from the pressure applied in the epoxy resin. However, in cell D, the cork's behavior when pressured limited its operation. In fact, the cork still exhibits a compression margin and, because it is a granulate material, behaves differently than the cork without pressure. One possible modification could be the substitution of this material for pure cork, or a thinner granulate, less compressible.

Calibration

The demodulation of plantar and shear pressures was achieved, with more evident results in sensing cell A. It was obtained sensitivities between 0.56 and 2.16 pm/kPa for normal pressure and between 0.51 and 3.98 pm/kPa, for horizontal pressure. Comparing these

values with those encountered in literature, it is confirmed that they are within the range of sensitivity previously reported in studies of Koulaxouzidis *et al*, who reached sensitivity values of 2.2 pm/kPa for normal pressure and 1.3 pm/kPa for shear/diagonal pressure [54].

However, some errors may have been introduced in the calibration and, as possible improvement, it is suggested performing future calibrations using machines of automated compression, with extended ranges, in order to guarantee a continuous compression (not stepwise, as used in this work), to ensure the maximum similarity of the calibration method between sensor cells and to reduce positioning errors. Also, bidirectional shear calibration may be useful to check if the response of the sensing cells to both directions of the shear pressure is the same, in the anterior-posterior axis.

Optical fibers

The process of inscribing FBGs contributes to the inherent fragility of optical fibers. In fact, in the insole manufacturing process, the dimensions of the fiber guides and sensing cells, must be meticulously calculated, in order to perfectly match, causing the least strain on the fiber. Unwanted strain will induce noise in the signal acquired by the interrogation system and consequently, introduce errors in the analysis of foot pressures. The most critic paths are between consecutive sensing cells, where the fiber is fixed by the epoxy resin. In fact, some of the errors observed may have been introduced by the tension applied to the fiber when bending the insole during walking.

New insole configurations may suggest an architecture with fiber guides with a specific design, so that the fiber is looser, preventing the stretch in the limits of plantar and dorsi-flexion movements.

Cork insoles

Although not presented in this work, sensing insoles with two optical fibers – for cells A, B, and C – were constructed to overcome the problem with the curvature of the fiber, after sensor cell 3. In these insoles, some signal disturbances were observed from the bending of the insole, without any pressure applied in the sensing cells. This is a tremendously limiting factor in the normal use of the insoles since, ideally, the insole should be inert to any kind of contribution from the natural bending of the human foot during gait.

Although these effects were not observed in the original insole (presented in this work), some changes were devised for a future optimization of the prototype. Thus, it is suggested the replacement of the middle layer (layer 2), originally made of epoxy resin, by a cork sheet. In addition, a 1.5 mm gap around the sensing cells and between the several parts where the cells were placed (**Figure 5.1**).

(a) **(b)**

Figure 5.1 – **(a)** New insole configuration. **(b)** Layer 2 made from a cork sheet, cut by CO_2 laser.

This layer can be easily obtained by CO_2 laser cut process. Thus, the insole adapts to a greater variability of movements of the normal walking, allowing the isolation of the FBGs' signal, intended for measurement of the plantar and shear pressures.

Two prototypes of this insole were fabricated with sensing cell A and D installed. However, due to time constraints, these were not fully tested yet.

Moreover, and considering that the bending of the insoles may result in a pressure applied in the bottom part of the insole – thus triggering the FBG wavelength shift – a vertical air gap between the bottom layer and the epoxy resin cell may be introduced.

e-Health systems

The results obtained by the sensor insoles emphasize the assumption of these as a viable solution for e-Health and dynamic monitoring systems. The insole proposed in this work would be part of a mobile e-Health system for continuous monitoring of plantar and shear pressures, in patients with gait disorders. This non-invasive solution comprises the sensing element, described and tested in this work; the interrogation system and finally, the mobile app. The interrogator, an expensive tool in this system, allows the recording of Bragg wavelength for subsequent conversion to pressure values. The mobile app would be a versatile tool, capable of being installed on a computer or mobile phone with wireless connection, where the monitoring results obtained by the sensors and presenting stats that can be consulted over a period. The system would be capable to transfer the continuously measured data to a cloud, allowing the health professionals to easily consult the patient performance, to elaborate a more consistent analysis, according to the displayed results.

Publications

During this dissertation, a scientific paper entitled "Gait Shear and Plantar Pressure Monitoring: A Non-Invasive OFS Based Solution for e-Health Architectures" was published at MDPI Sensors journal in April of 2018. Doi: 10.3390/s18051334.

Also, a book chapter entitled "Fiber Bragg Gratings as e-Health enablers: an overview for gait analysis applications", was submitted in Application of Optical Fibre for Sensing, IntechOpen, London, United Kingdom, 2018.

References

[1] W. J. Jeffcoate and K. G. Harding, "Diabetic Foot Ulcers", *The Lancet*, vol. 361, pp. 1545-1551, 2003.

[2] B. E. Sumpio, "Foot Ulcers", *The New England Journal of Medicine*, pp. 787–793, 2000.

[3] A. Veves, H. J. Murray, M. J. Young and A. J. Boulton, "The Risk Of Foot Ulceration In Diabetic Patients With High Foot Pressure: A Prospective Study", *Diabetologia*, vol. 35, no. 7, pp. 660–663, 1992.

[4] L. Shu, T. Hua, Y. Wang, Q. Qiao Li, D. D. Feng, and X. Tao, "In-Shoe Plantar Pressure Measurement And Analysis System Based On Fabric Pressure Sensing Array", *IEEE Transactions On Information Technology In Biomedicine*, vol. 14, no. 3, pp. 767–775, 2010.

[5] T. W. Kernozek, E. E. Lamott, and M. J. Dancisak, "Reliability Of An In-Shoe Pressure Measurement System During Tredmill Walking", *Foot & Ankle International,* pp. 204–209, 2016.

[6] M. N. Orlin and T. G. McPoil, "Plantar Pressure Assessment", *Physical Therapy*, vol. 80, no. 4, pp. 399–409, 2000.

[7] R. M. Queen, A. N. Abbey, J. I. Wiegerinck, J. C. Yoder, and J. A. Nunley, "Effect Of Shoe Type On Plantar Pressure: A Gender Comparison", *Gait Posture*, vol. 31, no. 1, pp. 18–22, 2010.

[8] W. Aerts *et al.*, "Validation Of Plantar Pressure Simulations Using Finite And Discrete Element Modelling In Healthy And Diabetic Subjects", *Compututer Methods In Biomechanics and Biomedical Enginneering*, vol. 20, no. 13, pp. 1442–1452, 2017.

[9] G. Agrawal, *Nonlinear Fiber Optics*, 3rd ed. San Diego, CA: Academic Press, 2001.

[10] T. Marasovič, M. Cecič, and V. Zanchi, "Analysis And Interpretation Of Ground Reaction Forces In Normal Gait", *WSEAS Transactions on Systems*, vol. 8, no. 9, pp. 1105–1114, 2009.

[11] I. A. De Quervain, S. R. Simon, S. Leurgans, W. S. Pease, D. McAllister, and I. A. Kramers De Quervain, "Gait Pattern In The Early Recovery Period After Stroke", *The Journal of Bone And Joint Surgery*, vol. 78, no. 10, pp. 1506–1514, 1996.

[12] National Diabetes Data Group, "Classification And Diagnosis Of Diabetes Mellitus And Other Categories Of Glucose Intolerance", *Diabetes,* vol. 28, no. December, pp. 1039–1057, 1979.

[13] American Diabetes Association, "Definition And Description Of Diabetes Other Categories Of Glucose", *Diabetes Care*, vol. 33, 2010.

[14] J. P. Assal, I. Muhlhauser, A. Pernet, R. Gfeller, V. Jorgens, and M. Berger, "Patient Education As The Basis For Diabetes Care In Clinical Pratice And Research", *Diabetologia*, pp. 602–613, 1985.

[15] W. C. Wang, W. R. Ledoux, B. J. Sangeorzan, and P. G. Reinhall, "A Shear And Plantar Pressure Sensor Based On Fiber-Optic Bend Loss", *Journal of Rehabilitation Research & Development*, vol. 42, no. 3, p. 315, 2005.

[16] J. Z. Hao, K. M. Tan, S. C. Tjin, C.Y. Liaw, P. Roy Chaudhuri, X. Guo, and C. Lu, "Design Of A Foot-Pressure Monitoring Transducer For Diabetic Patients Based On FBG Sensors", *16th Annual Meeting IEEE Lasers Electro-Optics Society*, vol. 1, pp. 23–24, 2003.

[17] R. A. Sage, J. K. Webster, and S. G. Fisher, "Outpatient Care And Morbidity Reduction In Diabetic Foot Ulcers Associated With Chronic Pressure Callus", *Journal Of The American Podiatric Medical Association*, vol. 91, no. 6, pp. 275–279, 2001.

[18] R. Lobmann *et al.*, "Effects Of Preventive Footwear On Foot Pressure As Determined By Pedabarography In Diabetic Patients: A Prospective Study", *Diabetic Medicine*, vol. 18, pp. 314-319, 2001.

[19] S. M. Marshall, "Prevention And Early Detection Of Vascular Complications Of Diabetes", *The BMJ*, vol. 333, no. 7566, pp. 475–480, 2006.

[20] A. J. M. Boulton, L. Vileikyte, G. Ragnarson-tennvall, and J. Apelqvist, "Review The Global Burden Of Diabetic Foot Disease", *The Lancet*, vol. 366, pp. 1719–1724, 2005.

[21] N. Singh, D. G. Armstrong, and B. A. Lipsky, "Preventing Foot Ulcers", *Journal Of The American Podiatric Medical Association*, vol. 293, no. 2, pp. 94–96, 2005.

[22] C. A. Abbot, A. P. Garrow, A. L. Carrington, J. Morris, E. R. Van Ross, A. J. Boulton, "Foot Ulcer Risk Is Lower In South-Asian And African-Carribean Compared With European Diabetic Patients In The U.K.", *Diabetes Care*, vol. 8, no. 8, pp. 1869–1875, 2005.

[23] J. S. Steinberg, M. Edmonds, D. P. Hurley, and W. N. King, "Confirmatory Data From EU Study Supports Apligraf For The Treatment Of Neuropathic Diabetic Foot Ulcers", *Journal Of The American Podiatric Medical Association*, vol. 100, no. 1, pp. 73–7, 2010.

[24] J. Apelqvist, G. Ragnarson-Tennvall, and J. Larsson, "Long-Term Costs for Foot Ulcers in Diabetic Patients in a Multidisciplinary Setting", *Foot & Ankle International*, vol. 16, no. 7, pp. 388–394, 1995.

[25] E. S. Sazonov, G. Fulk, N. Sazonova, and S. Schuckers, "Automatic Recognition Of Postures And Activities In Stroke Patients", *31st Annual International Conference of the IEEE Engineering in Medicine and Biology Society, EMBC 2009*, pp. 2200–2203, 2009.

[26] M. F. Domingues, N. Alberto, C. Leitão, C. Tavares, E. Rocon de Lima, A. Radwan, V. Sucasas, J. Rodriguez, P. André, and P. Antunes, "Insole Optical Fiber Sensor Architecturefor Remote Gait Analysis - An eHealth Solution", *IEEE Internet Of Things Journal*, vol. 4662, no. c, 2017.

[27] M. F. Domingues, N. Alberto, C. Leitão, P. André, E. Rocon de Lima, A. Radwan, V. Sucasas, J. Rodriguez, and P. Antunes, "An Insole Optical Fiber Sensor Architecture For Plantar Pressure Monitoring", *Journal Of Biomedical Optics,* pp. 1–6, 2017.

[28] M. F. Domingues, C. Tavares, C. Leitão, A. Frizera-Neto, N. Alberto, C. Marques, A. Radwan, J. Rodriguez, O. Postolache, E. Rocon, P. André, and P. Antunes, "Insole Optical Fiber Bragg Grating Sensors Network For Dynamic Vertical Force Monitoring", *Journal of Biomedical Optics*, vol. 22, no. 9, p. 091507, 2017.

[29] R. M. Queen, B. B. Haynes, W. M. Hardaker, and W. E. Garrett, "Forefoot Loading During 3 Athletic Tasks" *The American Journal Of Sports Medicine*, vol. 35, no. 4, pp. 630–636, 2007.

[30] K. T. V. Grattan and T. Sun, "Fiber Optic Sensor Technology: An Overview" *Sensors and Actuators*, vol. 82, no. 1–3, pp. 40–61, 2000.

[31] B. Lee, "Review Of The Present Status Of Optical Fiber Sensors" *Optical Fiber Technology*, vol. 9, no. 2, pp. 57–79, 2003.

[32] A. D. Kersey, "A Review Of Recent Developments In Fiber Optic Sensor Technology", *Optical Fiber Technology*, vol. 2, pp. 291–317, 1996.

[33] A. H. Razak, A. Zayegh, R. K. Begg, and Y. Wahab, "Foot Plantar Pressure Measurement System: A Review", *Sensors*, vol. 12, no. 7, pp. 9884–9912, 2012.

[34] B. A. MacWilliams and P. F. Armstrong, "Clinical Applications Of Plantar Pressure Measurement In Pediatric Orthopedics", *Pediatric Gait: A New Millennium In Clinical Care And Motion Analisys Technology*, pp. 143–150, 2000.

[35] H. S. Zhu, J. J. Wertsch, G. F. Harris, J. D. Loftsgaarden, and M. B. Price, "Foot Pressure Distribution During Walking And Shuffling", *Archives Of Physical Medicine and Rehabilitation*, vol. 72, no. 6, pp. 390–397, 1991.

[36] H. Zhu, N. Maalej, J. G. Webster, W. J. Tompkins, P. Bach-Y-Rita, and J. J. Wertsch, "An Umbilical Data-Acquisition System for Measuring Pressures between the Foot and Shoe", *IEEE Transactions On Biomedical. Engineering*, vol. 37, no. 9, pp. 908–911, 1990.

[37] J. J. Wertsch, J. G. Webster, and W. J. Tompkins, "A Portable Insole Plantar Pressure Measurement System", *Journal Of Rehabilitation Research and Development,* 1992.

[38] J. M. Hausdorff, Z. Ladin, and J. Y. Wei, "Footswitch System For Measurement Of The Temporal Parameters Of Gait", *Journal of Biomechanics*, vol. 28, no. 3, pp. 347–351, 1995.

[39] T. L. Lawrence and R. N. Schmidt, "Wireless In-shoe Force System", *Proceedings of the 19th Annual International Conference of IEEE Engineering in Medicine and Biology Society*, vol. 19, no. C, pp. 2238–2241, 1997.

[40] C. M. Yang, C. M. Chou, J. S. Hu, S. H. Hung, C. H. Yang, C. C. Wu, M. Y. Hsu, and T. L. Yang, "A Wireless Gait Analysis System By Digital Textile Sensors", *Proceedings of the 31st Annual International Conference of IEEE Engineering in Medicine and Biology Society,* pp. 7256-7260, 2009.

[41] S. M. M. De Rossi, T. Lenzi, N. Vitiello, M. Donati, A. Persichetti, F. Giovacchini, F. Vecchi, M. C. Carrozza, "Development Of An In-Shoe Pressure-Sensitive Device For Gait Analysis", *Proceedings of the 33rd Annual International Conference of IEEE Engineering in Medicine and Biology Society,* pp. 5637–5640, 2011.

[42] S. M. M. De Rossi, N. Vitiello, T. Lenzi, R. Ronsse, B. Koopman, A. Persichetti, F. Giovacchini, F. Vecchi, A. J. Ijspeert, H. van der Kooij, M. C. Carrozza, "Soft Artificial Tactile Sensors For The Measurement Of Human-Robot Interaction In The Rehabilitation Of The Lower Limb", *Proceedings of the 32nd Annual International Conference of IEEE Engineering in Medicine and Biology Society,* pp. 1279–1282, 2010.

[43] S. M. M. De Rossi, N. Vitiello, T. Lenzi, R. Ronsse, B. Koopman, A. Persichetti, F. Vecchi, A. J. Ijspeert, H. van der Kooij, M. C. Carrozza, "Sensing Pressure Distribution On A Lower-Limb Exoskeleton Physical Human-Machine Interface", *Sensors*, vol. 11, no. 1, pp. 207–227, 2011.

[44] T. Lenzi, N. Vitiello, S. M. M. De Rossi, A. Persichetti, F. Giovacchini, S. Roccella, F. Vecchi, M. C. Carrozza, "Measuring Human-Robot Interaction On Wearable Robots: A Distributed Approach", *Mechatronics*, vol. 21, no. 6, pp. 1123–1131, 2011.

[45] S. J. M. Bamberg, A. Y. Benbasat, D. M. Scarborough, D. E. Krebs, and J. a Paradiso, "Gait Analysis Using A Shoe-Integrated Wireless Sensor System", *IEEE Transactions On Information Technology in Biomedicine*, vol. 12, no. 4, pp. 413–23, 2008.

[46] S. R. Edgar, T. Swyka, G. Fulk, and E. S. Sazonov, "Wearable Shoe-Based Device For Rehabilitation Of Stroke Patients", *Proceedings of the 32nd Annual International Conference of IEEE Engineering in Medicine and Biology Society,* pp. 3772–3775, 2010.

[47] A. Querido, M. P. Castro, J. P. Vilas-Boas, R. Corredeira, D. Daly, and R. J. Fernandes, "Reliability And Accuracy Of Spatial-Temporal Gait Parameters Measured By The Walkinsense®", *Proceedings Of Institution Of Mechanical Engineers, Part P: Journal Of Sports Engineering and Technology*, vol. 230, no. 4, pp. 275–279, 2016.

[48] F. Yong, G. Yunjian, and S. Quanjun, "A Human Identification Method Based On Dynamic Plantar Pressure Distribution", *Proceedings of the IEEE Internatinal Conference on Inforation and Automation*, no. June, pp. 329–332, 2011.

[49] T. Yamakawa, K. Taniguchi, K. Asari, S. Kobashi, and Y. Hata, "Biometric Personal Identification Based On Gait Pattern Using Both Feet Pressure Change", *Proceeding 2010 World Automation Congress*, pp. 1–6, 2010.

[50] M. Lord, R. Hosein, and R. B. Williams, "Method For In-Shoe Shear Stress Measurement", *Journal Of Biomedical Engineering*, vol. 14, no. 3, pp. 181–186, 1992.

[51] J. W. Tappin, J. P. Pollard, and E. A. Beckett, "Method Of Measuring Shearing Forces On The Side Of The Foot", *Clinical Physics and Physiological Measurement*, vol. 1, pp. 83–85, 1980.

[52] F. Akhlaghi and M. G. Pepper, "In-Shoe Biaxial Shear Force Measurement: The Kent Shear System", *Medical & Biological Engineering & Compututing*, vol. 34, no. 4, pp. 315–317, 1996.

[53] G. T. Kanellos, G. Papaioannou, D. Tsiokos, C. Mitrogiannis, G. Nianios, and N. Pleros, "Two Dimensional Polymer-Embedded Quasi-Distributed FBG Pressure Sensor For Biomedical Applications", *Optics Express*, vol. 18, no. 1, pp. 179–186, 2010.

[54] A. V. Koulaxouzidis, M. J. Holmes, C. V. Roberts, and V. A. Handerek, "A Shear And Vertical Stress Sensor For Fibre Bragg Gratings", *Proceedings of the 22nd Annual International Conference of IEEE Engineering in Medicine and Biology Society*, vol. 1, no. 1980, pp. 55–58, 2000.

[55] Z. F. Zhang, X. M. Tao, H. P. Zhang, and B. Zhu, "Soft Fiber Optic Sensors For Precision Measurement Of Shear Stress And Pressure" *IEEE Sensors Journal*, vol. 13, no. 5, pp. 1478–1482, 2013.

[56] Y. J. Rao, "Recent Progress In In-Fibre Bragg Grating Sensors", *Optics and Lasers in Engineering*, vol. 31, pp. 297–324, 1999.

[57] K. O. Hill, Y. Fujii, D. C. Johnson, and B. S. Kawasaki, "Photosensitivity In Optical Fiber Waveguides: Application To Reflection Filter Fabrication", *Applied Physics Letters*, vol. 32, no. 10, pp. 647–649, 1978.

[58] W. Liang, Y. Huang, Y. Xu, R. K. Lee, and A. Yariv, "Highly Sensitive Fiber Bragg Grating Refractive Index Sensors", *Applied Physics Letters*, vol. 86, no. 15, pp. 1–3, 2005.

[59] S. Yin and P. Ruffin, "Fiber Optic Sensors", *Wiley Encyclopedia Of Biomedical Engineering*, pp. 225–285, 2006.

[60] A. Ghatak and K. Thyagarajan, *An Introduction To Fiber Optics*. Cambridge University Press, 1998.

[61] G. P. Agrawal, *Applications of Nonlinear Fiber Optics*. San Diego, CA: Academic Press, vol. 55, no. 6. 2002.

[62] K. O. Hill, B. Malo, F. Bilodeau, D. C. Johnson, and J. Albert, "Bragg Gratings Fabricated In Monomode Photosensitive Optical Fiber By UV Exposure Through A Phase Mask", *Applied Physics Letters*, vol. 62, no. 10, pp. 1035–1037, 1993.

[63] C. J. S. De Matos, P. Torres, L. C. G. Valente, W. Margulis, and R. Stubbe, "Fiber Bragg Grating (FBG) Characterization And Shaping By Local Pressure", *Applied Physics Letters.*, vol. 19, no. 8, pp. 1206–1211, 2001.

[64] A. Othonos, "Fiber Bragg Gratings", *American Institute Of Physics*, vol. 68, no. 12, 1997.

[65] J. Crisp, *Introduction To Fiber Optics,* 2nd ed. Oxford: Newnes, 2001.

[66] E. Udd and W. B. Spillman, *Fiber Optic Sensors - An Introduction for Engineers and Scientists,* 2nd ed. Hoboken, New Jersey: John Wiley & Sons, Inc, 2011.

[67] M. F. S. Ferreira, *Óptica E Fotónica*. Lisboa: Lidel, 2003.

[68] A. D. Kersey, M. A. Davis, H. J. Patrick, M. LeBlanc, K. P. Koo, C. G. Askins, M. A. Putnam, and E. J. Friebele, "Fiber Grating Sensors", *Journal Of Lightwave Technology,* vol. 15, no. 8, pp. 1442–1463, 1997.

[69] Y. Shen, J. Xia, T. Sun, and K. T. V. Grattan, "Photosensitive Indium-Doped Germano-Silica Fiber For Strong Fbgs With High Temperature Sustainability", *IEEE Photonics Technology Letters*, vol. 16, no. 5, pp. 1319–1321, 2004.

[70] H. Venghaus, *Wavelength Filters in Fibre Optics*, Springer, 2006.

[71] U. Sampath, H. Kim, D. Kim, Y. Kim, and M. Song, "*In-Situ* Cure Monitoring Of Wind Turbine Blades By Using Fiber Bragg Grating Sensors And Fresnel Reflection Measurement", *Sensors*, 2015.

[72] J. Yang, X. Dong, Y. Zheng, K. Ni, C. C. Chan, and P. P. Shum, "Magnetic Field Sensing With Reflectivity Ratio Measurement Of Fiber Bragg Grating", *Sensors*, 2014.

[73] L. F. Ferreira, P. Antunes, F. Domingues, P. A. Silva, and P. S. André, "Monitoring Of Sea Bed Level Changes In Nearshore Regions Using Fiber Optic Sensors", *Measuremet: Journal Of The International Measurement Confederation*, vol. 45, no. 6, pp. 1527–1533, 2012.

[74] A. Zhang, B. Guan, X. Tao, and H. Tam, "Experimental And Theoretical Analysis Of Fiber Bragg Gratings Under Lateral Compression", *Optics Communications* vol. 206, no. May, pp. 81–87, 2002.

[75] H. Kogelnik and C. V. Shank, "Stimulated Emission In A Periodic Structure", *Applied Physics Letters*, vol. 18, no. 4, p. 152, 1971.

[76] D. Grobnic, C. W. Smelser, S. J. Mihailov, and R. B. Walker, "Long-Term Thermal Stability Tests At 1000 °C Of Silica Fibre Bragg Gratings Made With Ultrafast Laser Radiation", *Measurement Science and Technology*, vol. 17, no. 5, pp. 1009–1013, 2006.

[77] N. J. Alberto, L. M. B. Bilro, P. F. da Costa Antunes, C. S. J. Leitão, H. F. J. Lima, P. S. de Brito André, J. de Lemos Pinto, "Optical Fiber Technology for eHeathcare", in *Handbook Of Research On Icts And Management Systems For Improving Efficiency In Healthcare And Social Care*, IGI Global, vol. I, 2013.

[78] S. P. Silva, M. A. Sabino, E. M. Fernandes, V. M. Correlo, L. F. Boesel, and R. L. Reis, "Cork : Properties, Capabilities And Applications", *Journal International Materials Review,* vol. 6608, 2013.

[79] W. D. Callister, *Fundamentals Of Materials Science And Engineering*, 5th ed. John Wiley & Sons, Inc., 2001.

[80] J. P. Davim and A. G. Magalhães, *Ensaios Mecânicos E Tecnológicos*, 3rd ed. Publindústria, 2010.

[81] J. T. M. Cheung, M. Zhang, A. K. L. Leung, and Y. B. Fan, "Three-Dimensional Finite Element Analysis Of The Foot During Standing - A Material Sensitivity Study", *Journal Of Biomechanics*, vol. 38, no. 5, pp. 1045–1054, 2005.

[82] K. Tao *et al.*, "An In Vivo Experimental Validation Of A Computational Model Of Human Foot", *Journal of Bionic Engineering*, vol. 6, no. 4, pp. 387–397, 2009.

[83] W. M. Chen, T. Lee, P. V. S. Lee, J. W. Lee, and S. J. Lee, "Effects Of Internal Stress Concentrations In Plantar Soft-Tissue-A Preliminary Three-Dimensional Finite Element Analysis", *Medical Engineering & Physics*, vol. 32, no. 4, pp. 324–331, 2010.

[84] A. M. Lebar, G. F. Harris, J. J. Wertsch, and H. Zhu, F. Harris, "An Optoelectronic Plantar 'Shear' Sensing Transducer: Design, Validation and Preliminary Subject Tests", *IEEE Transactions On Rehabilitation Engineering*, vol. 4, no. 4, pp. 310–319, 1996.

[85] M. Lord and R. Hosein, "A Study Of In-Shoe Plantar Shear In Patients With Diabetic Neurophaty", *Clinical Biomechanics*, vol. 15, no. 1, pp. 46–53, 2000.

[86] R. Hosein and M. Lord, "A Study Of In-Shoe Plantar Shear In Normals", *Clinical Biomechanics*, vol. 15, no. 1, pp. 46–53, 2000.

[87] J. E. Perry, J. O. Hall, and B. L. Davis, "Simultaneous Measurement Of Plantar Pressure And Shear Forces In Diabetic Individuals", *Gait & Posture*, vol. 15, no. 1, pp. 101–107, 2002.

[88] D. Zou, M. J. Mueller, and D. J. Lott, "Effect Of Peak Pressure And Pressure Gradient On Subsurface Shear Stresses In The Neuropathic Foot", *Journal of Biomechanics*, vol. 40, no. 4, pp. 883–890, 2007.

[89] M. J. Mueller, D. Zou, K. L. Bohnert, L. J. Tuttle, and D. R. Sinacore, "Plantar Stresses On The Neuropathic Foot During Barefoot Walking", *Physical Therapy*, vol. 88, no. 11, pp. 1375-1384, 2008.

[90] D. J. Lott, D. Zou, and M. J. Mueller, "Pressure Gradient And Subsurface Shear Stress On The Neuropathic Forefoot", *Clinical Biomechanics*, vol. 23, no. 3, pp. 342–348, 2008.

[91] S. Rajala and J. Lekkala, "Plantar Shear Stress Measurements - A Review", *Clinical Biomechanics,*, vol. 29, no. 5, pp. 475–483, 2014.

[92] Y. Zhao and Y. Liao, "Discrimination Methods And Demodulation Techniques For Fiber Bragg Grating Sensors", *Optics And Lasers In Engineering*, vol. 41, no. 1, pp. 1–18, 2004.

[93] Y. Rao, "In-Fibre Bragg Grating Sensors", *Measurement Science and Technology,* vol. 355, 1997.